The Thesis Committee for Philip Hua Wang
Certifies that this is the approved version of the following thesis:

Analysis of Radio Controlled Airplane Landing Gear Using Empirical Similitude

APPROVED BY
SUPERVISING COMMITTEE:

Supervisor:

Richard H. Crawford

Raul Longoria

Analysis of Radio Controlled Airplane Landing Gear Using Empirical Similitude

by

Philip Hua Wang

Thesis

Presented to the Faculty of the Graduate School of

The University of Texas at Austin

in Partial Fulfillment

of the Requirements

for the Degree of

Master of Science in Engineering

The University of Texas at Austin

May 2018

Acknowledgements

I would like to thank my advisor, Dr. Crawford, for the wealth knowledge and support he provided throughout the 2 years. From airplanes to HVAC, you always know which questions to ask and which answers to define further. I have learned a lot about how to approach different problems from an engineering perspective from our discussions, and that is something I will take with me far into the future.

I would also like to thank Dr. Longoria for his insight, as this was invaluable to my work. Despite your busy schedule you made time wherever you could to help me along in my research.

To my mom and dad, I want to thank you for the unconditional moral and financial support that you provided for me during this time. It never matter what I needed, you were always there to support me. To my sister, thank you for standing by me during the highs and lows over the years.

Lastly, thank you to all my friends who have filled this journey with encouragement and fun.

Abstract

Analysis of Radio Controlled Airplane Landing Gear Using Empirical Similitude

Philip Wang, MSE

The University of Texas at Austin, 2018

Supervisor: Richard H. Crawford

This thesis uses empirical similitude to compare the drop test result of an RC plane landing gear to a large oleo strut landing gear. This is useful to help create novel designs for applications onto large aircraft, as it is difficult to run experiments on the larger system.

A drop test rig was constructed to collect data from an RC plane tire. The system is built similar to a reverse pendulum with the tire at the end of the arm. The accelerometer at the end of the arm records the acceleration, with the important results being the peak accelerations at the impacts. These were exported to Excel files to be read by MATLAB during analysis.

The second order ODE system derived from a mass-spring-damper model is coded into MATLAB and compared to empirical data. The code tracks the system as it falls, bounces on the ground, rises back in the air, and repeats, recording position, velocity, and acceleration predicted. The result was then compared to data from the drop test rig. A unitless matrix is derived relating the peak forces predicted by the ODE system to the peak forces of the actual data.

The second order system was then scaled up to a large oleo-pneumatic system, creating a matrix of physical parameters. The unitless matrix was applied to this new prediction plot to convert it to “real” data. The resultant plot is compared to empirical data to determine if force plots are comparable. In conclusion, empirical similitude was able to successfully predict peak amplitudes recorded by past literature, though more research is required to confirm accuracy of the results. Successful modeling of an oleo-strut system using an RC tire paves the way for modeling novel landing gear systems in the future.

Table of Contents

Acknowledgements iv

Abstract v

Table of Contents vii

List of Tables ix

List of Figures x

Chapter 1 Introduction 1

1.1 Problem Statement 2

1.2 Thesis Organization 2

Chapter 2 Literature Review 4

2.1 Background 4

2.2 The Traditional Similitude Method 6

2.2.1 Dimensional Analysis 6

2.2.2 Prediction Equations 6

2.2.3 Buckingham Pi 7

2.2.4 Models 8

2.2.5 Distorted Models 8

2.2.6 Dissimilar Models 9

2.3 The Empirical Similitude Method 9

2.4 Oleo Strut 11

2.5 Previous Work 15

2.6 Summary 17

Chapter 3 Experimental Setup 18

3.1 Rig Setup 18

3.2 Parameters 20

3.3 Accelerometer 22

3.4 LabVIEW 25

3.5 Data Acquisition 26

3.6 Summary 27

Chapter 4 Simulation 28

4.1 Background 28

4.2 The Mass Spring Damper System 29

4.3 Defining Variables and Experimental Data 32

4.4 The Bouncing System 33

4.5 Summary 36

Chapter 5 Data Collection 37

5.1 Experimental Parameters 37

5.2 Simplified Model 38

5.3 Scaled Up Simulation 43

5.4 Applying Empirical Similitude 45

5.5 Summary 49

Chapter 6 Discussion 50

Chapter 7 Conclusion 56

7.1 Recommendations 57

References 58

List of Tables

Table 1: Dimensions for example piston 14

Table 2: MIL-H-5606 fluid properties 15

Table 3: Pin functions of accelerometer.....24

Table 4: Diameter of non-loaded tire 37

Table 5: Height measurements of loaded tire 38

Table 6: Equivalent stiffness values.....38

Table 7: Tire stiffness and damping coefficients 42

Table 8: Peak ratios used for F scaling vector 43

Table 9: Parameter value ratios for G scaling vector.....44

List of Figures

Figure 1. Mission profile of an LCAAT System 5

Figure 2. Empirical similitude visualized, going from the model specimen to the product 11

Figure 3. Deflection vs. Load of different systems in the landing gear.....12

Figure 4. Load vs. displacement curve of an example drop test system.....13

Figure 5. Measured data and linear or trilinear model fits lines of a car suspension system 16

Figure 6. Coordinate system relative to table 18

Figure 7. Inverse pendulum model 19

Figure 8. Full experimental setup: 1. Tire attached to the drop system, 2. Accelerometer mounted on arm, 3. PVC lever arm, 4. 3D printed pivot joint, 5. Mass on end of system, 6. Tires to be tested, 7. Breadboard, 8. myDAQ used for data acquisition, 9. LabVIEW Code 20

Figure 9. Simply supported beam with a distributed load 21

Figure 10. Test rig top view with accelerometer 22

Figure 11. ±100 G crossbow accelerometer 23

Figure 12. Image of pin location corresponding to Table 3.....24

Figure 13. Wired MyDAQ with 1. AI 0- port connected to AGND, 2. AI 0+ port connected to the Z output port of the accelerometer, 3. ground port GDNG, and 4. 5 V power supply.....25

Figure 14. Block Diagram of data acquisition code 26

Figure 15. Drop position of the inverse pendulum 27

Figure 16. Ball ODE plot that tracks when the ball hits the ground.....28
Figure 17. Mass-spring-damper system.....29
Figure 18. Full bond graph of mass-spring-damper system 30
Figure 19. Simplified bond graph of mass-spring-damper system.....31
Figure 20. Velocity, Position, and Acceleration of the predicted bouncing tire motion 36
Figure 21. Voltage output of accelerometer as read by LabVIEW.....39
Figure 22. Experimental data and simulation data comparison of first tire.....40
Figure 23. Experimental data and simulation data comparison of second tire 41
Figure 24. Experimental data and simulation data comparison of third tire.....41
Figure 25. Experimental data and simulation data comparison of fourth tire 42
Figure 26. Predicted position, velocity, and force of the product system.....44
Figure 27. Simulation's predicted force response to dropped landing gear system 46
Figure 28. Full size system simulation and predicted force plots of the first tire 47
Figure 29. Full size system simulation and predicted force plots of the second tire 47
Figure 30. Full size system simulation and predicted force plots of the third tire 48
Figure 31. Full size system simulation and predicted force plots of the fourth tire 48
Figure 32. Full size system simulation and predicted force plots of the first tire for the first bounce.....51

Figure 33. Full size system simulation and predicted force plots of the first tire for the second bounce 52
Figure 34. Full size system simulation and predicted force plots of the first tire for the fourth bounce.....52
Figure 35. Full size system simulation and predicted force plots of the first tire for the fourth bounce.....53
Figure 36. Force vs. Time experimental data and simulation response of a full-size landing gear system 54

Chapter 1: INTRODUCTION

When designing novel systems for large aircraft, predicting how different parts will react is difficult, as it is both expensive and time consuming to construct a full-size prototype. To reduce both cost and time, a smaller system is sometimes constructed and tested. The results of the smaller system can be scaled to predict reactions of the full-size system, though care must be taken when scaling. Distortions and dissimilarities between models can cause results to be inaccurate if not properly accounted for.

One application of this is in a recent project in the United States Air Force Academy (USAFA) capstone course. For this project, the cadets are required in their final semester to apply all that they have learned the previous four years to design, create, and test a novel landing gear system. After completing the full design process, the landing gear they create will be applied to a 25 lb. drone and tested in takeoff and landing. It is difficult to know if the 25 lb. radio-controlled (RC) plane can be representative of a 2000 lb. bomber drone. The eventual application would be on low-cost attritable aircraft technology (LCAAT) currently being developed by the Air Force.

LCAAT systems are drones that are relatively cheap and built for short term use. This means that fatigue failure is not a consideration and allows for design alternatives to the standard landing gear of an oleo strut and tire. The idea is that in a war of attrition, having lower cost attack aircraft with no risk to American pilots will be useful against potential combatants (United, 2016). There have been previous studies attempting to replace traditional landing gear systems with novel systems like skids but there is limited

research in this field (Shrotri, 2008). Design alternatives, as hypothesized and tested by the cadets on RC planes, are only useful if the system and its reactions are predictable. While for traditional similitude methods this would be a daunting task, empirical similitude can be used instead to derive effective scaling matrices.

1.1 Problem Statement

It is difficult to test novel systems like landing gears on large aircraft, so they are often tested on smaller scaled models like RC planes. The hypothesis of this research is that prediction equations can be matched to actual data using the theory of empirical similitude to make performance estimates.

This research focuses on creating a model of the RC plane landing gear system in MATLAB. The model predicts the position, velocity, and acceleration of the landing gear system and allows for scaling by empirically derived matrices. To test the accuracy of the model, a simple drop test rig was set up to collect real time data and compared to the model. Properties from full-size landing gears found in literature were used to create a scaling matrix that relates the parameters of the RC landing gear to the parameters of the full-size landing gear. The model was then scaled based on this matrix and its accuracy compared to the full-size landing gear data.

1.2 Thesis Organization

Chapter 2 contains a literature review starting with some background of the application at hand. The Traditional and Empirical Similitude Methods are properly defined. There were some complications later on with the oleo strut, so some of its

parameters are laid out. The chapter concludes with some insight into previous work that was used as a basis of the reported research.

Chapter 3 focuses on the experimental setup, starting with a quick summary of the setup of the rig. The methodology for finding the parameters used to describe the bouncing system in the simulation is then depicted. Because the accelerometer setup is a little more involved, a description of the process is reported. Lastly, the LabVIEW code and data collection process are detailed.

Chapter 4 explains the MATLAB code used to simulate the bouncing system. The basis for the code is specified first, then the second order ODE of the system when it is in contact with the ground is described. The important variables and parameters are then defined and a general summary of the entire code of the bouncing system is outlined.

Chapter 5 combines all the previous chapters to perform data collection, starting with the empirically derived experimental parameters. The simplified model is described, followed by the scaled-up system model. Finally, empirical similitude is applied to adjust the scaled-up model.

Chapter 6 is a discussion of the data collected previously, providing analysis and interpretation of the results.

Chapter 7 concludes the thesis and provides recommendations for future work.

Chapter 2: Literature Review

2.1 Background

USAFA is a military Air Force base that is set up like a university where cadets undergo a process similar to a four-year undergraduate program. The final semester of the mechanical engineering branch allows their cadets to apply what they have learned over the previous 3.5 years in a capstone course. The cadets work in groups of four to solve defense-related design problems. One recent problem was the design of a novel landing gear system for a LCAAT drone (United, 2016).

LCAAT systems are designed to be low cost and last about 10 cycles. These systems are usually unmanned air vehicles (UAV), or drones, used during war of attrition as cheap, replaceable alternatives to manned fighter jets. The low cycles to failure specification removes any fatigue restrictions. Since the systems are remotely controlled vehicles, there is more flexibility in requirements for pilot comfort and control. With fatigue and human conditions removed, more options for launch and recovery are feasible, and cost becomes the most important criterion. Figure 1 shows the general mission profile of an LCAAT drone (Risma, 2016).

Launching transitions the drone from a nonflying state to a flying state, while recovery transitions the drone from a flying state to a nonflying state. Recovery is normally more challenging to design for, as it is necessary for the aircraft to follow a specified approach path at a certain speed while taking wind and other factors into consideration. There must also be enough energy dissipated to bring the drone to rest

both horizontally and vertically relative to the landing platform (Gundlach, 2014). For this reason, the main focus of the work was on the recovery, or landing process, of the drone.

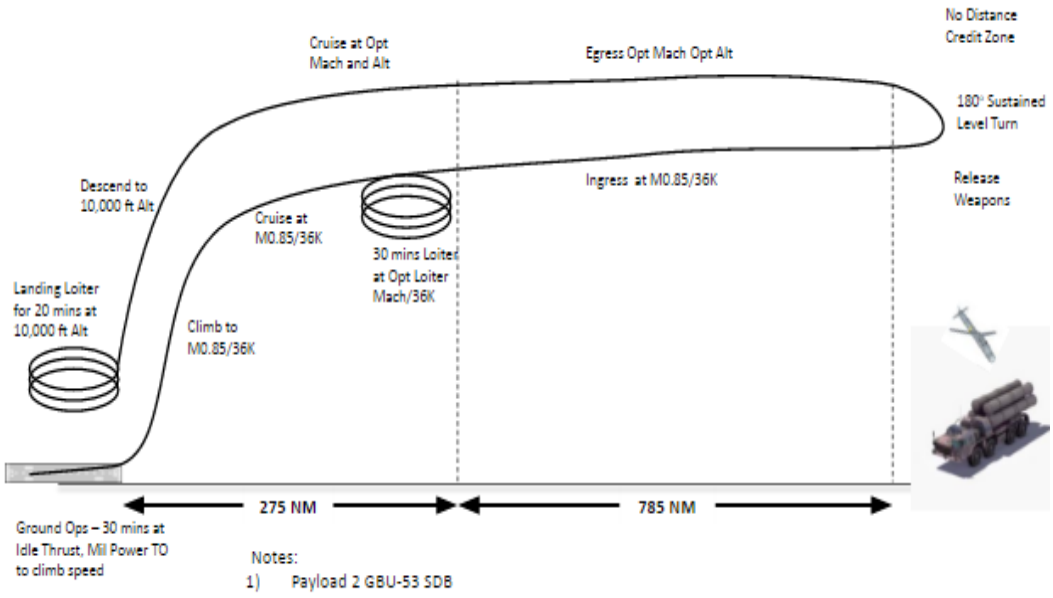

Figure 1. Mission profile of an LCAAT System (Risma, 2016).

Conventional launch and recovery used for large aircrafts involve a wheel and damper on a runway. This is the most common method for systems about 1000 lbs and above (Gundlach, 2014). The cadets focused on a 2000 lb B-12 bomber UAV (Risma, 2016). They were tasked with finding an alternative launch and recovery method that ideally will have a lower cost than the conventional method.

It is infeasible for the cadets to test their ideas on the full-size plane. Instead, they were tasked with building a system for a 25 lb RC plane. The goal is to then scale the reactions from the 25 lb drone to the 2000 lb drone using similitude.

2.2 THE TRADITIONAL SIMILITUDE METHOD

2.2.1 Dimensional Analysis

Dimensional analysis is an analytical tool that involves reducing units to their most basic form of measurement to compare different parameters. To compare different systems using dimensional analysis, two statements must be true:

- Quantities can be related only if they have the same dimensions. For example, a length unit must be related to a length, not mass, time, or any other unit.
- The ratio of properties with comparable quantities are independent of the units. For example, the length and width of a rectangle will always have the same ratio assuming consistent units.

These two axioms allow qualitative relationships to describe quantitative results and create accurate prediction equations (Murphy, 1950).

2.2.2 Prediction Equations

Prediction equations are effective tools that can give engineers a better understanding of a system before they build or model it. There are two general methods used to develop prediction equations: the experimental method and the analytical method. The first uses careful experimental observations and measurements to develop relationships between significant variables. The second uses known equations of the laws of physics that have already established relations between significant variables. In either case, the key is that dimensional analysis uses all the terms to form dimensionless groups called Pi terms (Murphy, 1950). The base concept of Pi terms can be seen in Equation 1.

$$\pi_1 = F(\pi_2, \pi_3, \pi_4, \pi_5) \quad (1)$$

2.2.3 Buckingham Pi

The Buckingham Pi theorem states that the number of Pi terms in a system is equal to the number of quantities subtracted by the number of basic dimensions as seen in Equation 2.

$$s = n - b \quad (2)$$

where *s* is the number of Pi terms, *n* is the number of variables involved, and *b* is the number of basic dimensions in the equation. So, for example, the kinematic equation of a falling object has the general function form of Equation 3.

$$x = f(t, v, a) \quad (3)$$

Where there are four quantities: position (*x*), time (*t*), velocity (*v*), and acceleration (*a*), and two basic dimensions, distance and time. Position as a function of the other three variables can be described as in Equation 4.

$$x = C_\alpha v^{c1} a^{c2} t^{c3} \quad (4)$$

Where C_α is a constant.

Using dimensional analysis to create two unitless Pi terms (4 quantities – 2 dimensions = 2 Pi terms), Equation 5 results.

$$\frac{x}{vt} = C_\alpha \left(\frac{gt}{v}\right)^{c_1} \quad (5)$$

The constants c_2 and c_3 disappear in the dimensionless equation out of necessity to maintain the first requirement of dimensional analysis (Murphy, 1950).

2.2.4 Models

A model is any mathematical formulation that relates to a physical system, by which data collected from the model can be used to predict a physical system, usually a prototype. Assuming Equation 6 below represents the desired response of the model and Equation 7 represents the desired response of the prototype. Dividing the two gives a prediction equation, as shown in Equation 8.

$$\pi_1 = F(\pi_2, \pi_3, \dots \pi_s) \tag{6}$$

$$\pi_{1p} = G(\pi_{2p}, \pi_{3p}, \dots \pi_{sp}) \tag{7}$$

$$\frac{\pi_{1p}}{\pi_1} = \frac{G(\pi_{2p}, \pi_{3p}, \dots \pi_{sp})}{F(\pi_2, \pi_3, \dots \pi_s)} \tag{8}$$

A model is considered a "true" model if all the Pi terms are equal, meaning the model and prototype function the same way under the same conditions (Murphy, 1950).

2.2.5 Distorted Models

It is often impossible to satisfy every Pi term. When a Pi term is not equivalent, the model is considered distorted. As more and more Pi terms become distorted, it becomes more and more difficult to predict how the prototype will respond (Murphy, 1950). Sometimes simple distortion factors will correct for them but the amount of

distortion in each system must be known beforehand. This becomes an issue in complex systems and prototypes.

2.2.6 Dissimilar Models

There are situations where a dissimilar model is used to represent a system. One of the most well-known uses of these is using electrical RLC[1] circuits to represent mass-spring-damper systems, and vice versa (Murphy, 1950). Masses store kinetic energy similar to inductors, springs store potential energy similar to capacitors, and dampers dissipate energy similar to the resistors. While the project at hand does not change the system as drastically as relating a circuit to a vibrating mass, it does relate a simple linear damper to an oleo-pneumatic (hydraulic-pneumatic) strut so there will need to be some adaptations. It is difficult to determine exactly how the model fits an actual dropping system from the principles. A solution to this is to gather data empirically and then use the empirical similitude method.

2.3 The Empirical Similitude Method

Empirical similitude is a novel similitude method that attempts to reduce distortion when scaling systems. Instead of using dimensional analysis, it uses empirical data from simplified versions of the system to create scaling matrices (Dutson, 2002).

[1] A RLC circuit is an electrical circuit consisting of a resistor (R), an inductor (L), and a capacitor (C). The components can be connected in series or in parallel.

It is easiest to explain empirical similitude using an example. Suppose it is desired to find properties of a system with a complex shape and made of a material that is difficult to manufacture. This system is called the *product*. A *model specimen* with a simple shape and material that is easy to manufacture is created. Equivalent properties to the ones desired on the product are then determined on the model specimen.

The model specimen undergoes two different transformations, and experimental data are taken from both embodiments. A system, called a *model*, with complex geometry made from the simple material is created. Properties corresponding to the one desired on the product are determined on the model. Then, a transformation matrix, F, is created for the geometric scaling by transforming the properties from the model specimen to the model. Now, returning to the model specimen, a system with the simple geometry but difficult material, called the *product specimen*, is created. Once again, properties are determined and the properties from the model specimen are transformed to the product specimen to create a transformation matrix, S.

By concatenating the two transformation matrices *S* and *F*, the model specimen can be scaled to the product. It has been discovered that there is an associative property with these scaling matrices, or essentially, that the scaling matrices are independent of each other. Scaling first by matrix *S* will not affect how the system scales by matrix *F* (Dutson, 2002). Figure 2 demonstrates visually the example of empirical similitude.

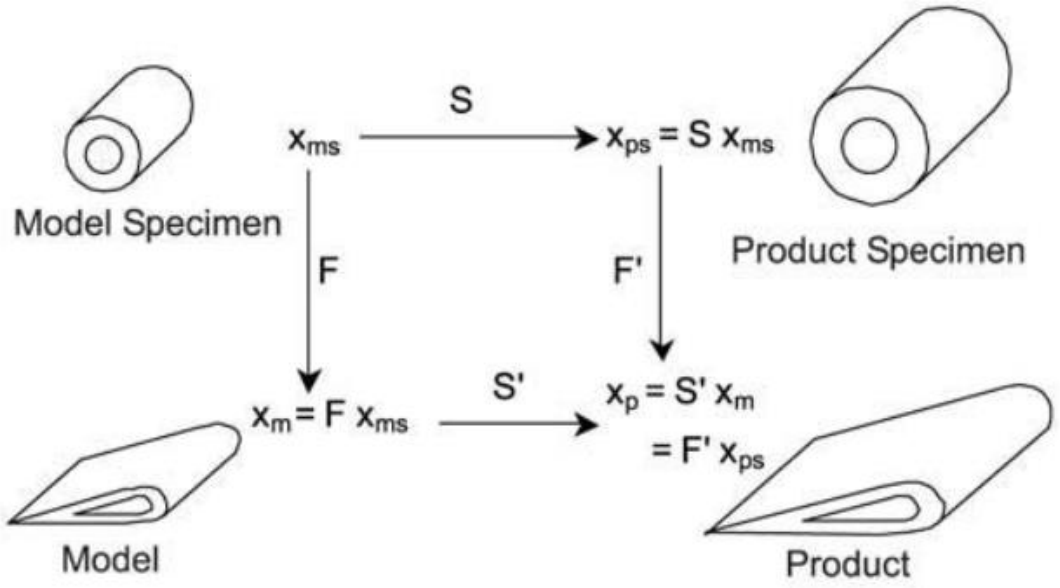

Figure 2. Empirical similitude visualized, going from the model specimen to the product (Dutson, 2002).

2.4 OLEO STRUT

The ultimate goal of the project is to scale a spring and tire to an oleo-pneumatic landing gear and tire.

An oleo-pneumatic strut is essentially a piston with air and oil that dissipates energy by forcing oil through an orifice. An ideal damper has no stiffness, meaning deflection and load should be independent (left plot in Figure 3). Unfortunately, ideal systems do not exist in the real world. In terms of deflection vs load though, the oleo-pneumatic system is one of the closest to ideal at dissipating energy as seen in Figure 3.

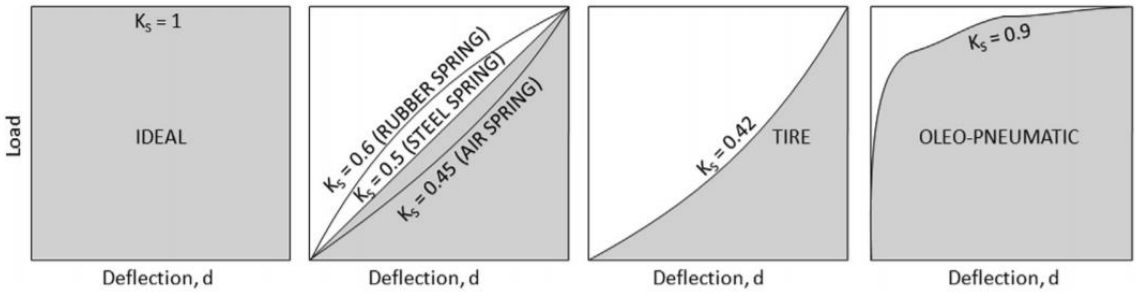

Figure 3. Deflection vs. Load of different systems in the landing gear (Gudmundsson, 2014).

This means that to minimize size and weight of the landing gear system, oleo-pneumatic struts should be used as shock absorbers of large loads (Gudmundsson, 2014).

During landing the wheel and thus the entire landing gear system are subject to drag and other forces due to a nonvertical tire impact on the runway. A drop test only loads the landing gear vertically. This means that shimmy and other potentially catastrophic factors are not considered during experiments (Davidson, 2015).

The air and oil in an oleo strut provide compliance and damping in the system. The load vs displacement curve can be used to determine the spring stiffness.

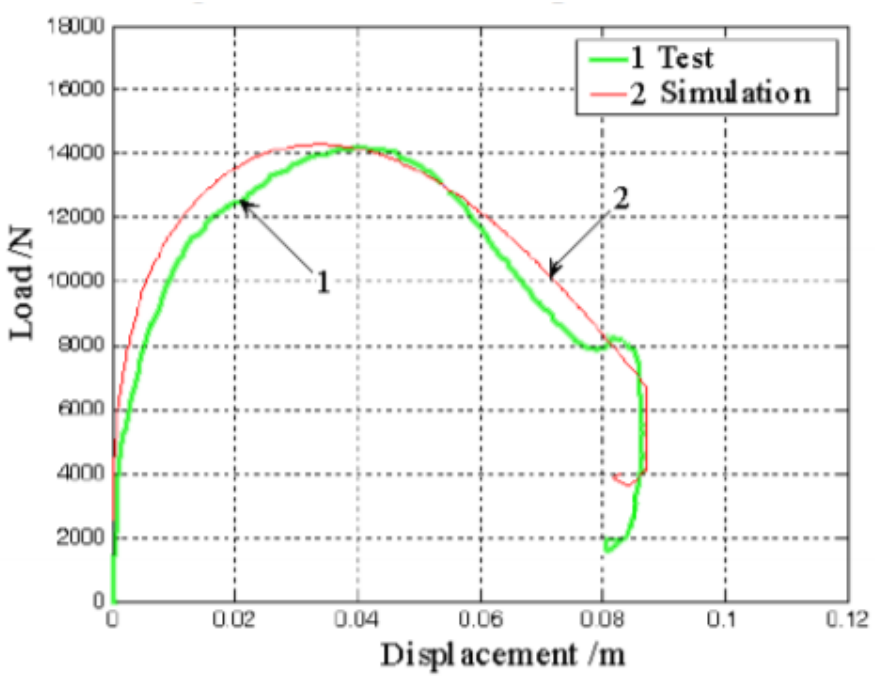

Figure 4. Load vs. displacement curve of an example drop test system (Yu, 2014).

For example, as seen in Figure 4, Yu et al. (2014) report that a peak load of 14000 N produces a displacement of 0.04 m in both experiments and in their simulation. Using Equation 9, the effective spring stiffness is calculated as k = 350000 N/m.

$$F_{spring} = kx \tag{9}$$

Damping force in a second order system is usually assumed to be linearly related to velocity. While this is a good assumption for many mechanical dampers, an oleo strut's damping is quadratic, while also keeping the sign of the original velocity. Damping force of an oleo strut can be seen in Equation 10.

$$F_h = 0.5\rho\left(A_y - A_z\right)V|V| \tag{10}$$

Where A_y is the piston surface area, A_z is the orifice surface area, and ρ is the fluid density. Assuming the quadratic relation with velocity, the other values combine to form the damping constant. Current landing gear system dimensions were used in this study, specifically the nose landing gear of the Model 99 Beechcraft. These piston dimensions can be found in Table 1.

Table 1. Dimensions for example piston (Khondker, 2009)

Beech craft Model 99		
Item	Nose landing gear	Main landing gear
Load at fully compressed position, lb	3,420	9,125
Piston outside diameter, in	1.7	2.7
Cylinder inside diameter, in	1.95	3.15
Total stroke, in	12	12
Total cylinder length, in	16.6	20

The oil most commonly used in the landing gears of Boeing airplanes is MIL-H-5606. This oil's density, which is required to find the damping force in Equation 10, can be found in Table 2.

Table 2. MIL-H-5606 fluid properties (Shell, 2012)

PROPERTIES	MIL-PRF-5606H	TYPICAL U.S. Production	European Production
Oil type	Mineral	Mineral	Mineral
Kinematic viscosity mm^2/s			
@ 100 °C	4.90 min	6.13	5.30
@ 40 °C	13.2 min	15.68	14.1
@ -40 °C	600 max	384	491
@ -54 °C	2500 max	1450	2300
Viscosity index	-	214	Over 200
Flashpoint Pensky Martin Closed Cup °C	82 min	104	105
Auto-ignition temperature °C	-	230	230
Pourpoint °C	-60 max	< -60	< -60
Total acid number mgKOH/g	0.20 max	0	0.01
Evaporation loss 6 hrs @ 71 °C %m	20 max	16.5	10
Water content ppm	100 max	55	<100
Relative density @ 15.6/15.6 °C	Report	0.874	0.87
Colour	Red	Red	Red
Particle contamination, number of particles per 100ml in size range			
5 to 15 microns	10000 max	1200	808
15 to 25 microns	1000 max	550	116
25 to 50 microns	150 max	70	44
50 to 100 microns	20 max	5	10
over 100 microns	5 max	0	1
Copper corrosion	2e max	1b	2b
Steel on steel wear scar diam mm	1.0 max	0.65	0.95

2.5 Previous Work

Studies have shown that pneumatic tire damping is difficult to model. This fact, in combination with the belief that other factors are more important, leads many studies to neglect tire suspension (Bauer, 2014). An analysis performed on a quarter car suspension system shows that accounting for tire damping reduced the percent error of the quarter car model from 17.8% to 10.7%. While 7% is not insignificant, tire damping is ignored in this research to focus on the dominant effects of the oleo strut (Maher, 2011).

The model drop system developed in this work, on the other hand, does not have enough weight to significantly deflect the coil spring, and so the spring had virtually infinite stiffness and was excluded from the analysis.

Analysis of a car suspension system shows that the quarter car's dampening factor is not linear, but trilinear as seen in Figure 5.

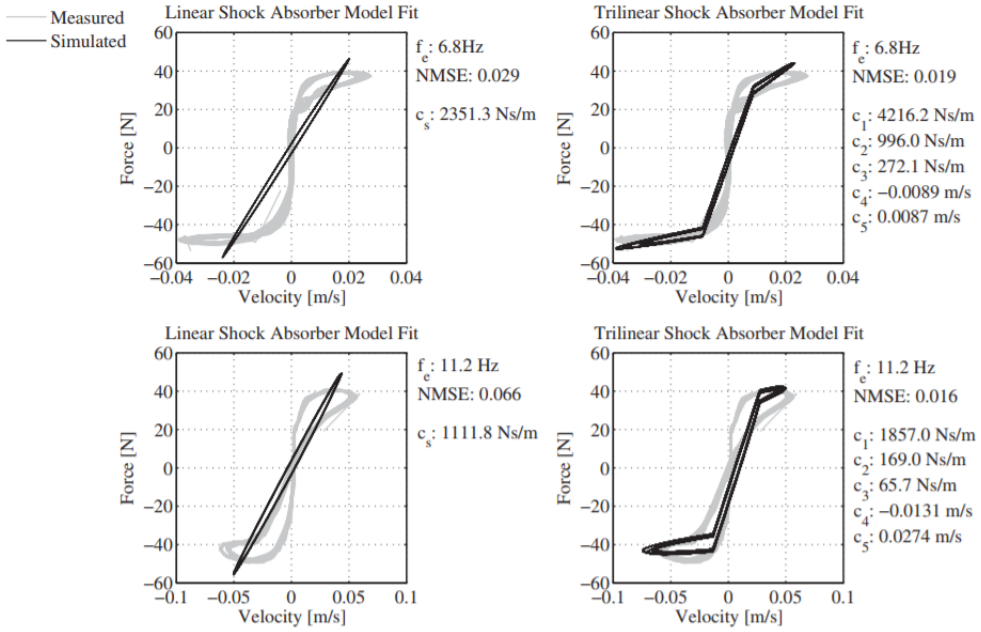

Figure 5. Measured data and linear or trilinear model fits lines of a car suspension system (Maher, 2011).

This model means that at large loads, the damping coefficient tends to overestimate the damping force, causing a simulation to overpredict the amount of damping force in the system. If it is assumed that the error increases with increasing force, the bouncing system's simulation plot can have lower peaks of maximum force

than the actual falling system. Ideally, this error will be accounted for with the scaling matrix calculation, but the conversion from a spring to a hydraulic damper may affect how well the system matches.

2.6 SUMMARY

In this chapter, past literature detailing the current application was explored to flesh out the problem statement described previously. Then, Traditional Similitude and Empirical Similitude Methods were properly defined to better understand scaling. Due to the difference in mathematical relations between mechanical and pneumatic dampers, the oleo-pneumatic damping system was further researched. Lastly, previous experiments done on suspension systems and landing gear systems were summarized to list out known sources of error and justify the assumptions made. The next chapter will present the experimental rig used to collect data of the model system.

CHAPTER 3: EXPERIMENTAL SETUP

To create an accurate unitless scaling matrix, a simple drop test experiment was performed. This involved constructing a test rig, collecting data, and matching that data to the simulation. The details of the experiments are provided in this chapter.

3.1 RIG SETUP

Before going into detail about the setup, a consistent coordinate frame must be defined. Sitting down in front of a table, the positive *z*-direction is vertical from the top of the table, the positive *x*-direction is to the right along the table, and the positive *y*-direction points away from the user. Figure 6 shows a visual representation of this coordinate system.

Figure 6. Coordinate system relative to table (All, 2002)

The drop test rig was designed to be simple and restrict motion to the *z*-direction. One way to do this involves a setup similar to the inverse pendulum, shown in Figure 7.

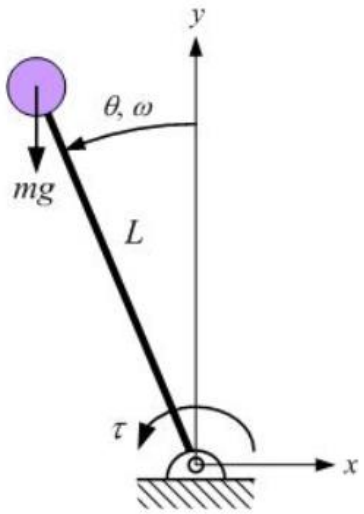

Figure 7. Inverse pendulum model (Kypuros, 2017)

The object to be dropped is bolted to an arm. The other end of the arm is attached to a grounded pin joint. This joint allows the arm to rotate freely about the *y*-axis, preventing motion in the *y*-direction and limiting motion in the *x*-direction to a fixed path. In this case, the object to be dropped is a 45 mm RC plane tire and the arm is a 20 mm diameter PVC pipe cut to 0.3 m. The pin joint consists of a steel pin press fit into a custom 3D printed joint of PLA plastic.

The joint was designed to easily fit the PVC pipe arm without rubbing against the walls to reduce the influence of friction. This joint is bolted to a 100 mm x 500 mm x 13 mm block of wood, grounding the joint. This block of wood was slightly narrow for the

joint but this did not affect attachment or tire landing consistency. After running the preliminary tests, it was apparent that the falling tire caused the entire rig to vibrate. To correct this, a large mass was attached at the end so that only the wheel and arm move after the impact. The full experimental setup can be seen in Figure 8.

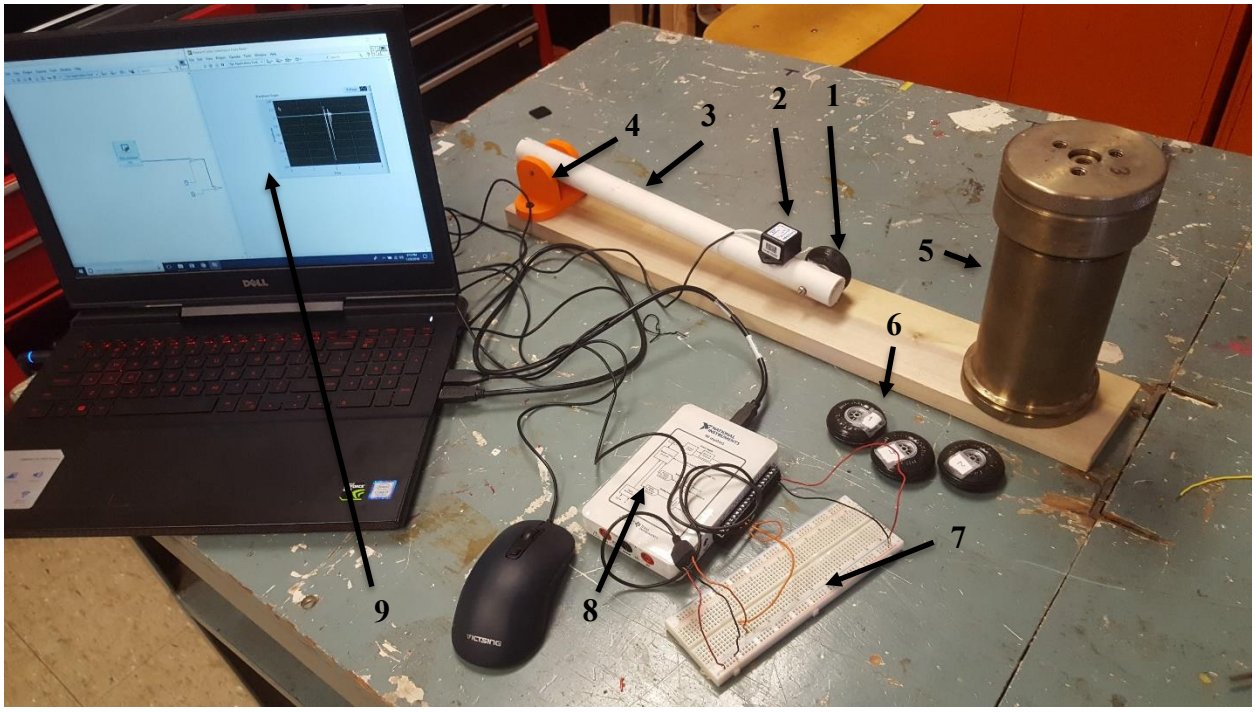

Figure 8. Full experimental setup: 1. Tire attached to the drop system, 2. Accelerometer mounted on arm, 3. PVC lever arm, 4. 3D printed pivot joint, 5. Mass on end of system, 6. Tires to be tested, 7. Breadboard, 8. myDAQ used for data acquisition, 9. LabVIEW Code

3.2 PARAMETERS

Since the goal of the experiments was to model the falling wheel as a falling mass-spring-damper system, parameters for mass and spring stiffness were found statically. Using a scale, the mass of each wheel was measured. The sensitivity of the scale was 0.001 kg, which is significant in the .01 kg system. However, the lever arm was

found to be .119 kg. Thus, the wheel is not the major component of mass, and so the potential error was disregarded. Because the wheel at the end does not support the entire weight of the lever arm the arm was modeled as a simply supported beam with the weight distributed over the length of the beam as shown in Figure 9.

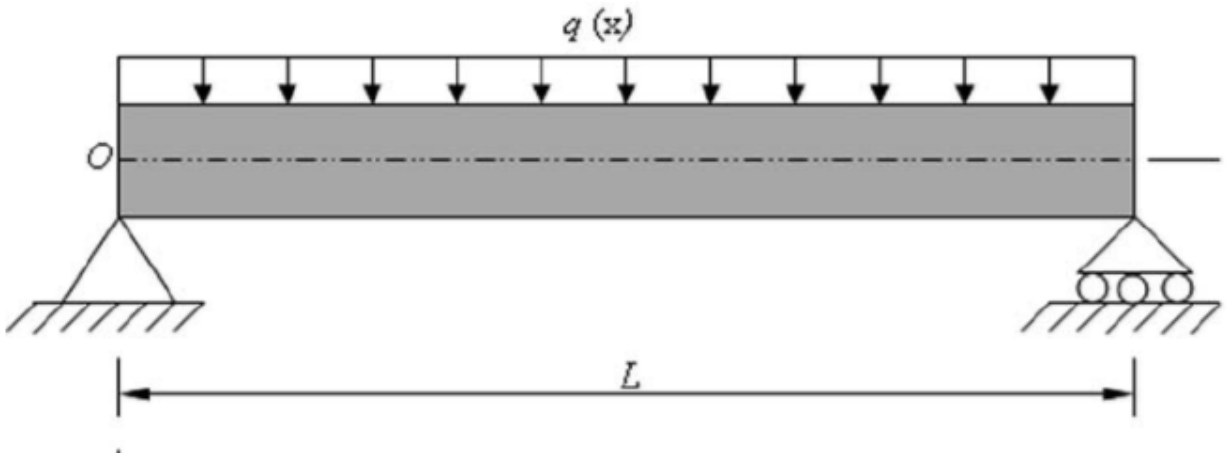

Figure 9. Simply supported beam with a distributed load (Sayyad, 2011)

The reaction force on the tire is half of the mass of the beam, and this was taken as the effective mass of the pipe. Adding these masses together, the effective mass is taken to be 0.07 kg. This value was confirmed with a scale placed at the impact point of the system.

The effective stiffness of the wheels was also determined statically. By hanging a known weight from the wheel, the deflection was measured using a caliper and a stiffness value was calculated. The wheel was placed on a plank that was hanging from a table and weighed on the other side. Tires tend to act linearly when tire deformation is small and

becomes more nonlinear with increased deformation (Maher, 2011). With the forces the RC plane tire will experience in the drop tests, the tire is not expected to deform a significant amount. Therefore, the stiffness of the tire will be assumed to be linear.

3.3 ACCELEROMETER

To collect data, a tri-axial accelerometer from Crossbow Technologies Inc. (CXL100HF3, Milpitas, CA, USA) is attached to the top of the pipe just above the tire using Velcro, as shown in Figure 10.

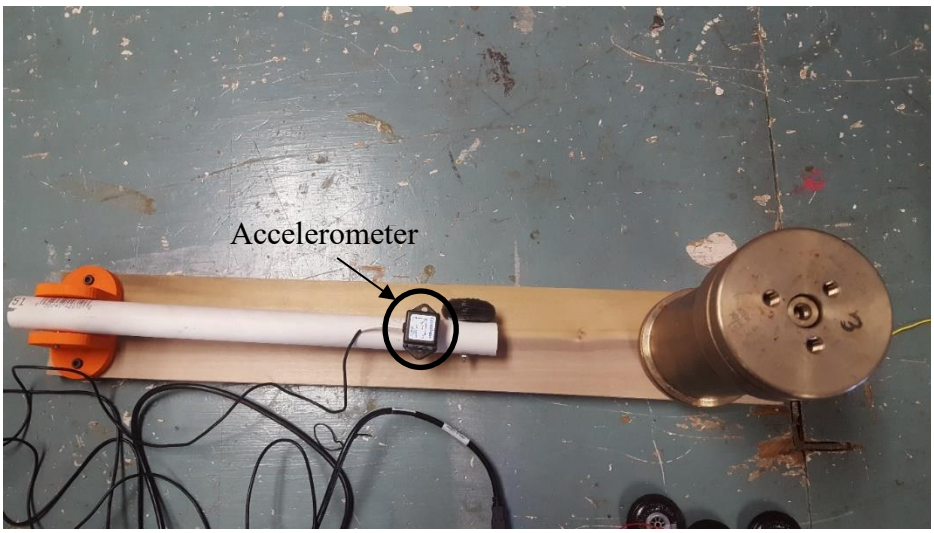

Figure 10. Test rig top view with accelerometer

This accelerometer has a 0-5 V output range with ±5G, ±10G, and ±100G potential acceleration ranges. The simulation (described in Chapter 4) results predicted the initial undamped impact accelerations to be around 80G. This drove the decision to use the 100G accelerometer. Figure 11 is a closeup image of the accelerometer used.

Figure 11. ±100 G Crossbow accelerometer

To ensure proper attachment of the flat-bottomed accelerometer to the round pipe, the arm was propped up by a bolt running through the bolt holes created and a flat was created using a drill. A bubble level was used to ensure that the flat is parallel to the bolt holes. A small square of Velcro hooks is glued to this square and the corresponding square of Velcro loops is glued to the bottom of the accelerometer. While this setup does allow for play in the x- and y- direction, most of this should be removed by the restricted motion limited by the hinge joint. Thus, the forces in those directions are considered negligible.

The accelerometer can be wired for data collection through National Instruments (Austin, TX, USA) myDAQ. A small breadboard was used to make connections. The

power in, ground, and z-axis out ports were connected from the accelerometer to the breadboard using the pin diagram seen in Table 3 and Figure 12.

Table 3. Pin functions of accelerometer (Crossbow, n.d.)

Pin	Color	Function
1	Red	Power In
2	Black	Ground
3	White	X-axis Out
4	Yellow	Y-axis Out
5	Green	Z-axis Out

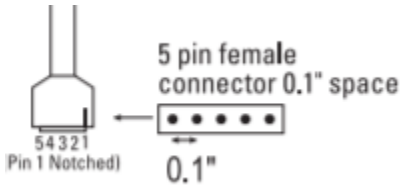

Figure 12. Image of pin location corresponding to Table 3 (Crossbow, n.d.)

Ports of interest on the myDAQ are the 5 V power supply and ground, and analog input (AI) ports. The 5 V power supply is connected in series with the power in of the accelerometer. The analog input 0+ port is connected in series to the z-axis output of the accelerometer. The 0- port of the analog input is grounded to AGND so that the reference voltage is 0 V. The DGND is connected to the ground of the accelerometer, completing the circuit. The hooked up MyDAQ can be seen in Figure 13.

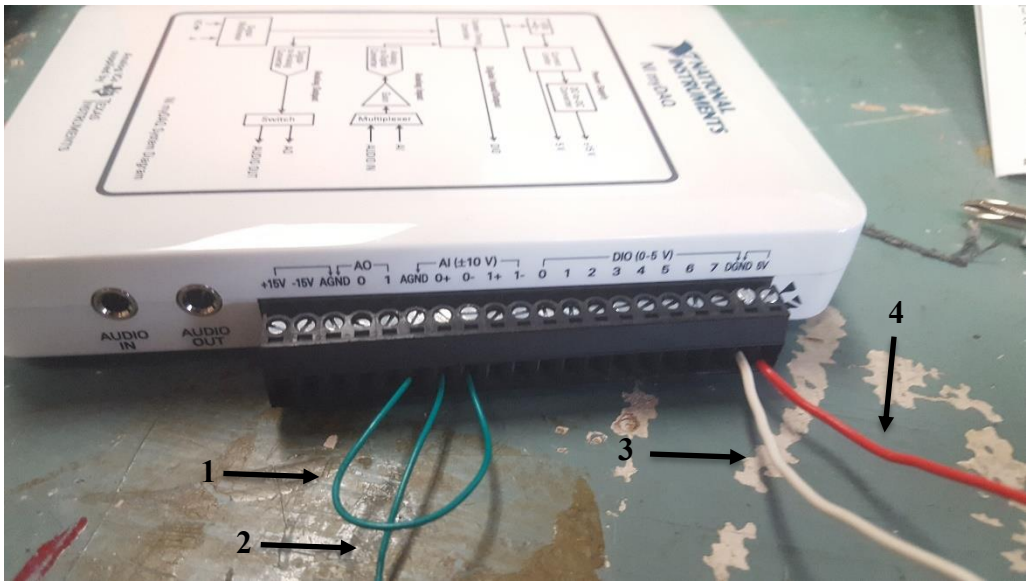

Figure 13. Wired MyDAQ with 1. AI 0- port connected to AGND, 2. AI 0+ port connected to the Z output port of the accelerometer, 3. ground port GDNG, and 4. 5 V power supply

3.4 LabVIEW

The driver in the myDAQ can automatically interface with National Instruments LabVIEW, and so this is the software of choice for reading the data. The accelerometer measures acceleration as a voltage varying from 0 V to 5 V. This voltage can be converted into a line plot with a simple write-to-measurement block connected to a waveform chart. The block diagram for the LabVIEW code can be seen in Figure 14.

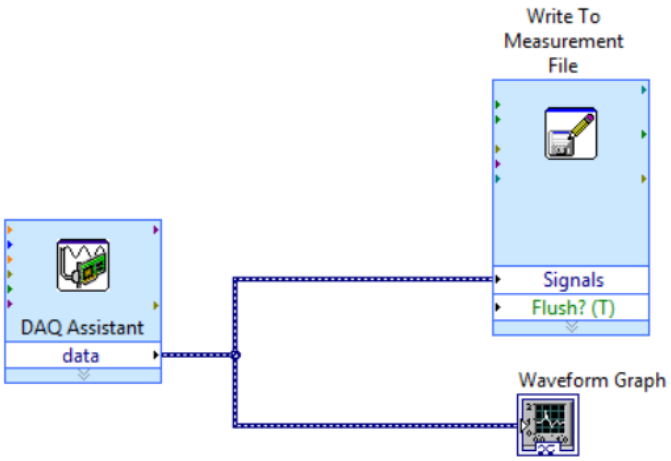

Figure 14. Block Diagram of data acquisition code.

The write-to-measurement block can then be output as an Excel file for easy access to each data point collected. The program was set to take data at a frequency of 1000Hz for 4 seconds, resulting in 4000 data points each experiment.

3.5 Data Acquisition

To acquire data, the arm was raised to its maximum height allowed by the hinge joint, as seen in Figure 15. The arm was then dropped from this position.

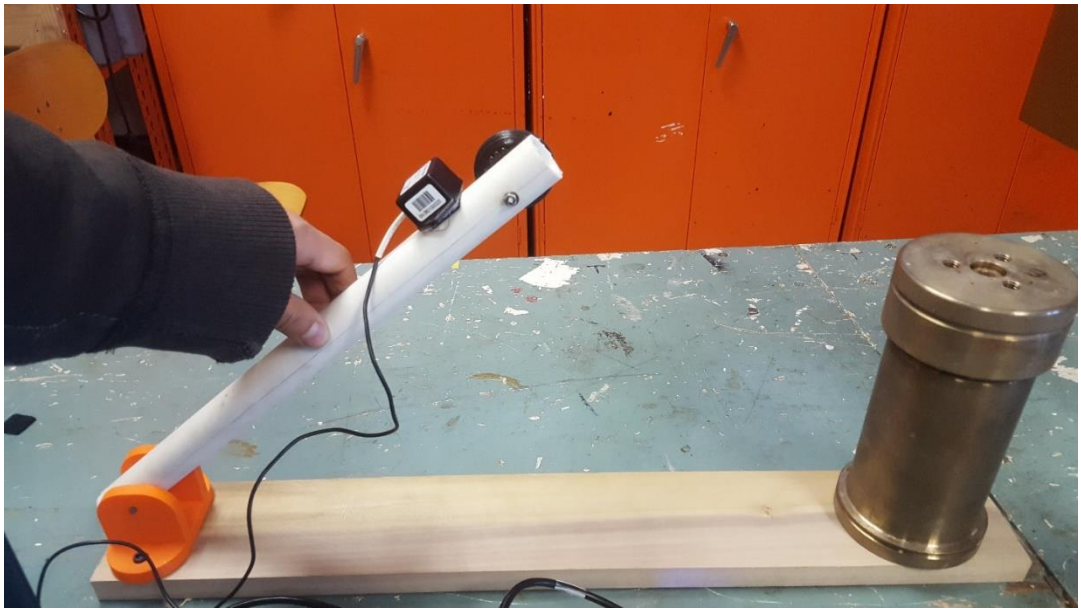

Figure 15. Drop position of the inverse pendulum.

The voltage output can be viewed from the waveform graph. After 5 trial runs to ensure repeatability, four wheels were dropped, and acceleration recorded 3 times, with the voltage values saved to Excel files.

3.6 SUMMARY

In this chapter, the experimental setup was explained in detail. The construction of the rig and initial parameters were established. Then, the accelerometer and data acquisition software associated with the accelerometer were detailed. Lastly, the drop test methodology was discussed. In the next chapter, the simulation model built with MATLAB code to track this drop test system will be described.

Chapter 4: Simulation

In this chapter, the simulation used to model the falling tire system is described in detail. The simulation was implemented using MATLAB (The MathWorks, Inc., Natick, MA, USA).

4.1 Background

The simulation code is loosely based on the "ballode" code provided with the MATLAB download package. The plot ballode returns can be seen in Figure 16. The ballode code tracks a ball by "throwing" a ball up in the air, tracking it until its position reaches 0, then changes its velocity to positive and removes some of the energy in the ball using a coefficient of restitution, in this case 0.9.

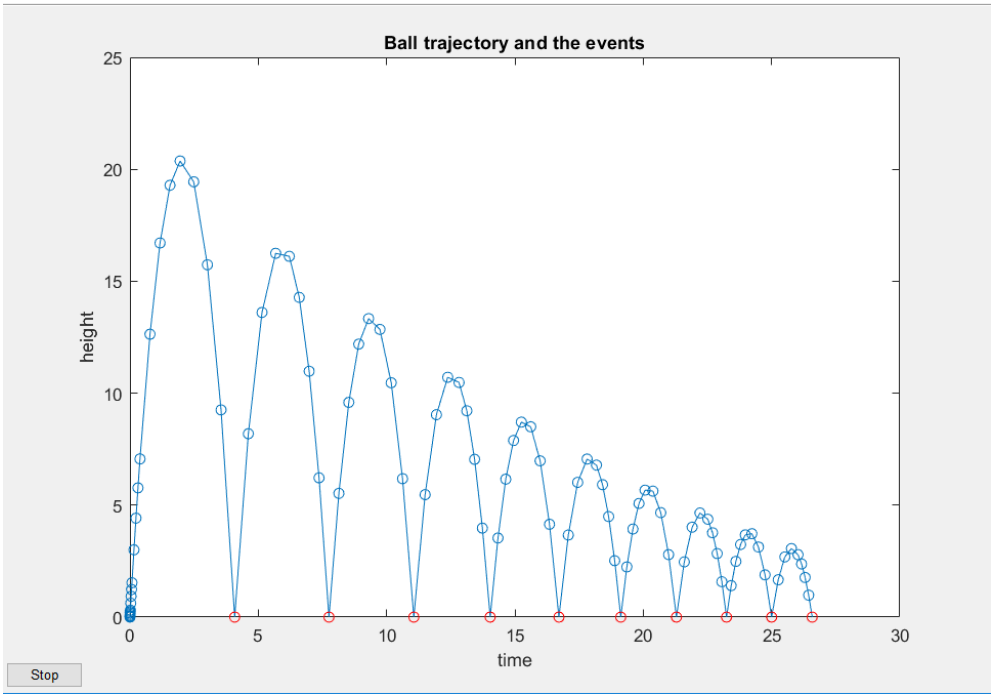

Figure 16. Ball ODE plot that tracks when the ball hits the ground

During each “bounce” the velocity is decreased by 10% and the ball is then tracked again until the next bounce where the process repeats for a set time period. The model of the falling tire uses this hybrid dynamic system, making transitions from a falling object system to a second order ordinary differential equation (ODE) mass-spring-damper system.

4.2 THE MASS-SPRING-DAMPER SYSTEM

When in contact with the ground, the system is modeled as a mass-spring-damper system, as seen in Figure 17.

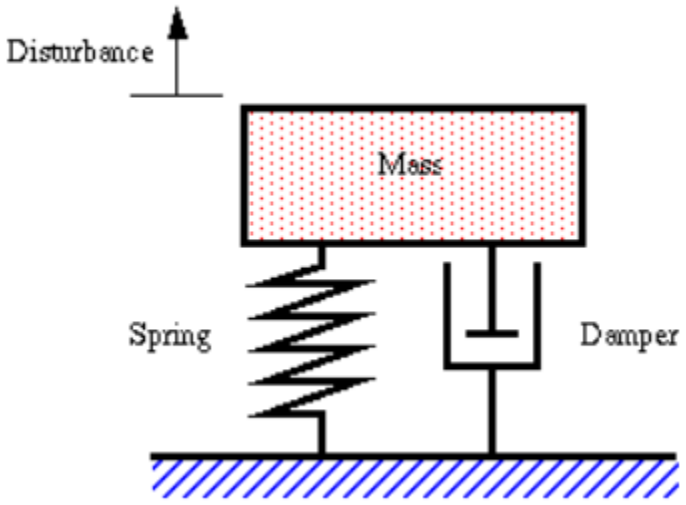

Figure 17. Mass-spring-damper system (Sutherland, 2011)

A bond graph is one way to derive the system equations. The bond graph can be seen in Figure 18.

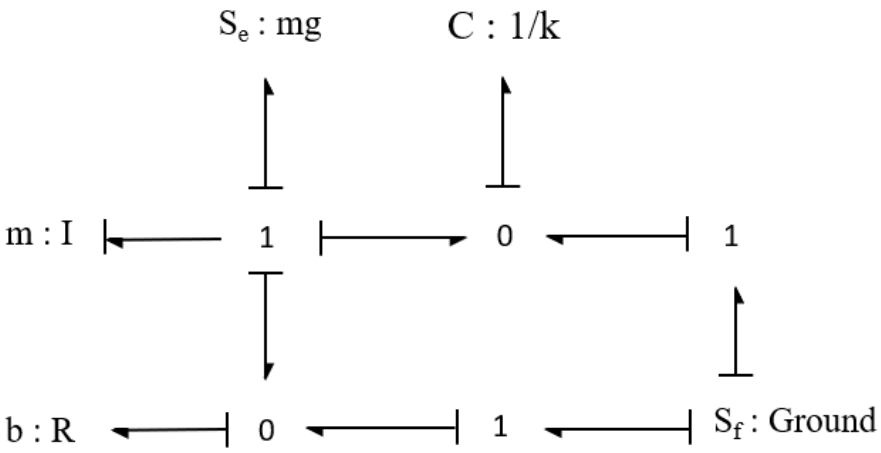

Figure 18. Full bond graph of mass-spring-damper system

The mass has a defined velocity, and so an inertial element (*m*) is attached to a common flow junction along with the force of gravity on the mass (S_g). Usually a source of effort would input power to the system, but due to the coordinate system with positive up, the force due to gravity is negative. Thus, the power flow goes into the source rather than the 1 junction. There is a differential velocity across the spring and damper, so two common effort ports merge the first common flow port, one with a capacitance element (*C*) representing the spring and the other with a resistance element (*R*) representing the damper. The ground has a defined velocity as well, so the two common effort junctions are each attached to another common flow junction, which is attached to a source of flow that is the ground. The bond graph can be simplified, as the velocity of the ground is zero. This means the lower common source port disappears. A two-junction port can be eliminated, as the effort and flow across a two-junction port are the same. This leaves just

a common flow port with a mass element, capacitance element, resistance element, and a source of effort attached to it, as seen in Figure 19.

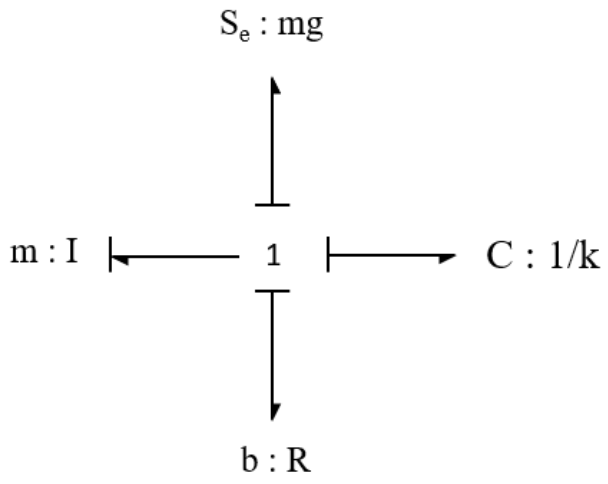

Figure 19. Simplified bond graph of mass-spring-damper system

The state equations can be derived from this bond graph. State variables are the momentum of the mass and the displacement of the spring, p and x respectively. To find the change in momentum, $\dot{p}$, of the mass, the sum of the efforts around the port is set equal to 0. Spring force is considered positive in extension, the force of gravity is considered negative as it is pointing down, and the damping force is only resistive and thus negative. Solving for $\dot{p}$, the equation becomes:

$$\dot{p} = -mg - kx - bv \tag{11}$$

where *v* is the velocity of the mass, $\dot{x}$. The change in displacement of the spring, $\dot{x}$, is proportional to the momentum of the mass.

$$\dot{x} = \frac{p}{m} \tag{12}$$

With these state equations developed, a MATLAB function was developed that takes inputs as the initial condition of the bond graph and that outputs the change in state.

4.3 Defining Variables and Experimental Data

This section describes the setup for the code. The empirically determined spring stiffness, effective mass of the system, gravity, and damping coefficient are set as global variables to be used in both the main code and the second order ODE solving function defined previously. The maximum height was measured to be 0.25 m. A time step, dt, of 0.001 seconds is the same as the data collection frequency used for the experiment. To predict the length of time over which the wheel will bounce on the ground, the damping ratio and natural frequency are calculated and used to find the damped frequency, as shown in Equations 13-15.

$$\zeta = \frac{b}{2\sqrt{km}} \tag{13}$$

$$w_n = \sqrt{\frac{k}{m}} \tag{14}$$

$$w_d = w_n\sqrt{1-\zeta^2} \tag{15}$$

The reciprocal of the damped frequency multiplied by 2π gives the period of the system.

$$T = \frac{2\pi}{w_d} \tag{16}$$

Acceleration data collected empirically with the drop test is in units of voltage and positive down, so simple algebra can convert the 0-5 V range to a -100 G to +100 G acceleration range with positive up. It is assumed that the data point when at rest and

falling is -1 G. The first few data points measured were back calculated to 101 G with a multiplier of 49.3, negated, and shifted back 100G.

$$a = -(V * 49.3 - 99) \tag{17}$$

These converted values were added to the acceleration plot alongside the acceleration predicted by the simulation.

4.4 BOUNCING SYSTEM

The simulation code begins with the tire at an initial height, then drops the system from rest. To simplify the model, instead of tracking the ball's position, the time over which the ball drops is calculated from the initial drop height. The only external force on the system is assumed to be gravity, so the time over which the first drop occurs can be seen in Equation 18.

$$t_{f1} = \sqrt{\frac{2h}{g}} \tag{18}$$

The time is then broken into 0.001 s increments and the corresponding position points over which the ball drops are calculated with kinematic equations.

$$y1 = h - 0.5g * t_1^2 \tag{19}$$

The velocity vector was solved iteratively using a `for` loop, as each velocity depends on the velocity of the previous frame.

$$v_{f1} = v_{i1} - g * dt^2 \tag{20}$$

When the position of the tire reaches 0, the dynamic system changes to a mass-spring-damper system. To accurately calculate the position and velocity during this time, a

second order ODE is solved using the function `rk4fixed`. This function is a 4th order Runge-Kutta numerical integrator that takes inputs of the state equations function, time span, initial conditions, and number of points and outputs vectors of state variables with a corresponding time vector.

For the inputs of `rk4fixed`, the starting time is equal to the final point in the previous time vector. Initially, the wheel is undeformed and just barely contacts the ground at position 0 m, with velocity of the final term of the previous velocity vector. Since the position point 0 is defined as the point where the spring is undeflected, the plot becomes negative while the spring is being compressed. To find the point where the system returns to position 0, a separate function was created called "Vibration.m" that tracks the mass-spring-damper system's oscillations specifically, without the dropping system. It uses the same `rk4fixed` code and parameter values and plots displacement and velocity vs time over multiple periods of the second order ODE. The first point over which the position changes from negative to positive (the 0 point) is extracted using the `find` command, and this is used as the time increment of the bounce system code.

The state variables function, called "bounceeq", is essentially a coded version of the model from the bond graph mentioned previously. The code requires two inputs: a time stamp and a vector of state variable values at the given time stamp. It then outputs the change in state variables as defined by the state equations at that time stamp.

New time, velocity, and position vectors are created combining the three vectors of the initial wheel in air with the corresponding three vectors found from the ODE of the

bounce. Then, the system-in-air methodology is repeated, calculating a final time using kinematics once again and creating a time vector in increments of the time step defined above. While conducting experiments, the wheel's acceleration only peaked significantly three times. Following this, the falling-bouncing sequence was iterated two more times until it also had three bounces. Each time, new time, position, and velocity vectors are created by combining the current iteration's vectors with the previous vector iterations.

At the end of the third bounce, for continuity purposes, another in-air iteration was performed, as it is safe to assume that the wheel rests on the ground with acceleration of -1 G. Finally, an acceleration vector is created by iteratively subtracting each velocity term from the previous one and dividing by the time step. There are now position and velocity vectors to plot against the time vector. The acceleration vector is one term shorter than the time vector. To convert the acceleration to G's, each value is divided by the gravity constant.

$$a(i) = \frac{v(i+1)-v(i)}{g*dt} \tag{21}$$

The plots of the system with mass of 0.070 kg, spring coefficient of 9400 N/m, and damping coefficient of 0 is shown in Figure 20.

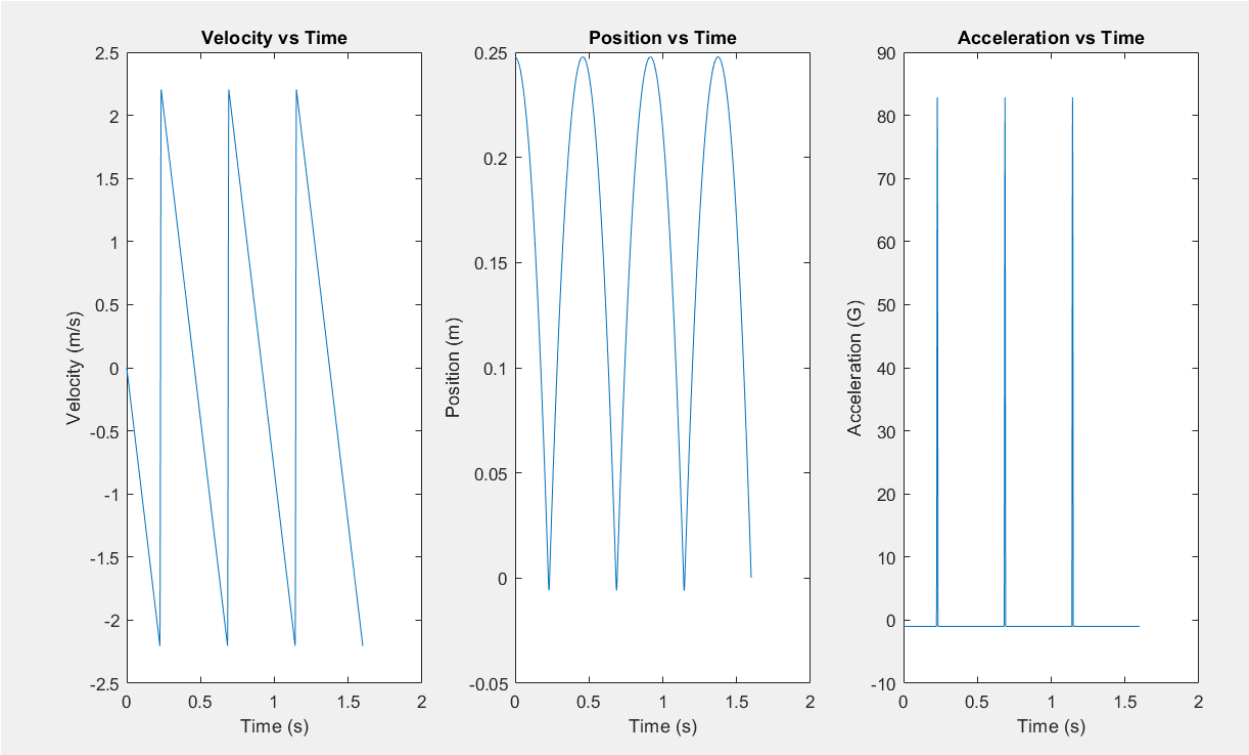

Figure 20. Velocity, Position, and Acceleration of the predicted bouncing tire motion

4.5 SUMMARY

In this chapter, the code used to track the falling tire and predict the acceleration of the bouncing system was detailed. First, the bouncing ball code that MATLAB provides was described, as the tracking system used was essential to the creation of the code. Then, the state equations were defined using the bond graph of a mass-spring-damper system. Lastly, important parameters and the model of interest were fleshed out. Now that the experimental rig is set up and the simulation code is tracking the tire's motion, data collection can begin.

Chapter 5: DATA COLLECTION

This chapter presents and analyzes the data that were acquired using the experimental setup and simulation model.

4.1 EXPERIMENTAL PARAMETERS

Before discussing the results of the simulation and experiment, it was necessary to find the stiffness of the tires that were being dropped. Four different tires were used in this experiment, and each of the tires were measured 3 times, generating an average diameter for each tire as seen in Table 4.

Table 4. Diameter of non-loaded tire

Unweighted Diameter (m)	tire			
test	1	2	3	4
1	0.0455	0.0453	0.0449	0.0453
2	0.0453	0.0452	0.0449	0.0452
3	0.0456	0.0454	0.0448	0.0450
Average	0.0455	0.0453	0.0449	0.0452

A weight was then hung from the tires, and the height of the tire was then measured. Due to increased chance of variance, five values were taken per tire and an average calculated, as seen in Table 5.

Table 5. Height measurements of loaded tire

Weighted Height (m)	tire			
	1	2	3	4
test				
1	0.0445	0.0447	0.0438	0.0442
2	0.0446	0.0445	0.0439	0.0444
3	0.0444	0.0446	0.0439	0.0444
4	0.0445	0.0446	0.0439	0.0444
5	0.0445	0.0446	0.0438	0.0444
Average	0.0445	0.0446	0.0439	0.0444

Knowing that the weight tested has a mass of 0.579 kg, which when converted to force is 5.68 N, the stiffness of the tire was then calculated. Table 6 shows the approximate spring stiffness values.

Table 6. Equivalent stiffness values

Tire	1	2	3	4
K (N/m)	5530	7760	5780	7150

There seems to be two distinct stiffness values between the four tires, and it is unclear exactly why this is the case. To maximize accuracy, all four tires were tested, developing different damping constants and conversion matrices for each.

5.2 SIMPLIFIED MODEL

Starting with the simplified model, the most important parameter to match is the time of the second bounce which is necessary for determining the damping coefficient. Figure 21 is one of the data plots taken from the experimental setup described in Chapter 3.

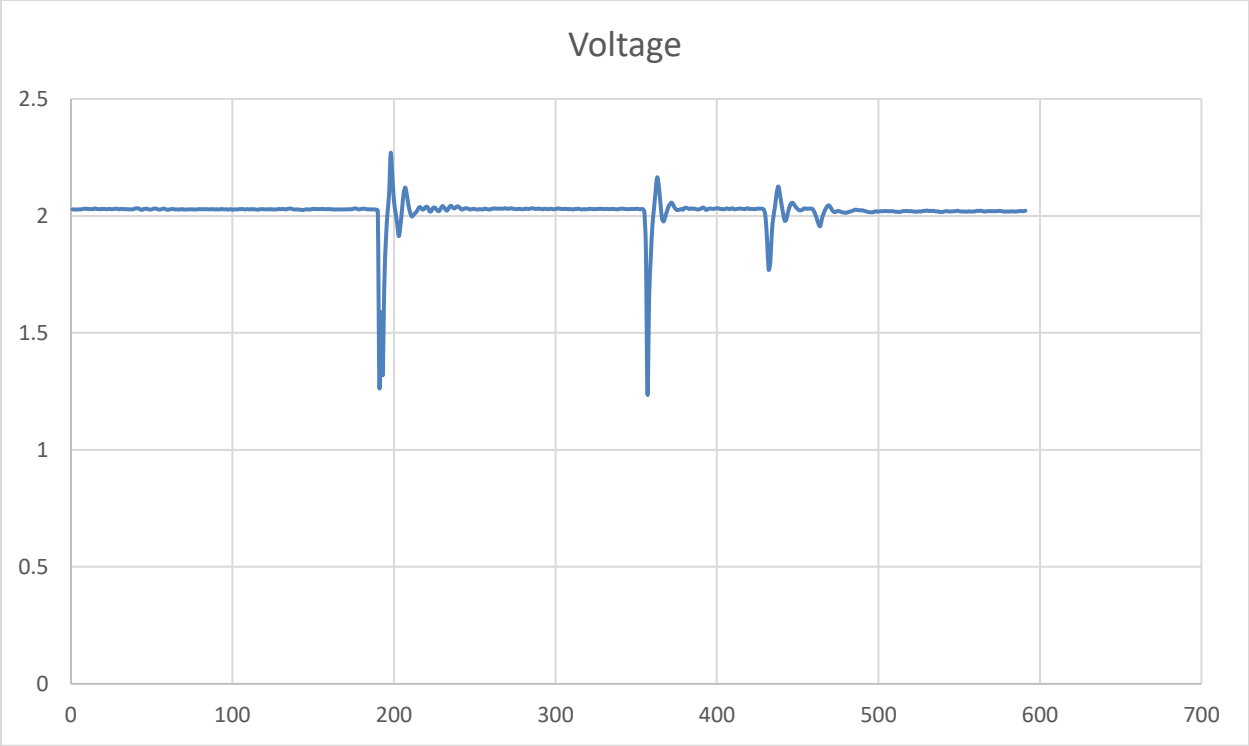

Figure 21. Voltage output of accelerometer as read by LabVIEW

Converting the units to force and matching the results to the simulation model, a damping factor of 15.0 N*s/m was determined to be the closest match to the data. Converting both the simulation and the data to force, the two plots can be compared, as seen in Figure 22.

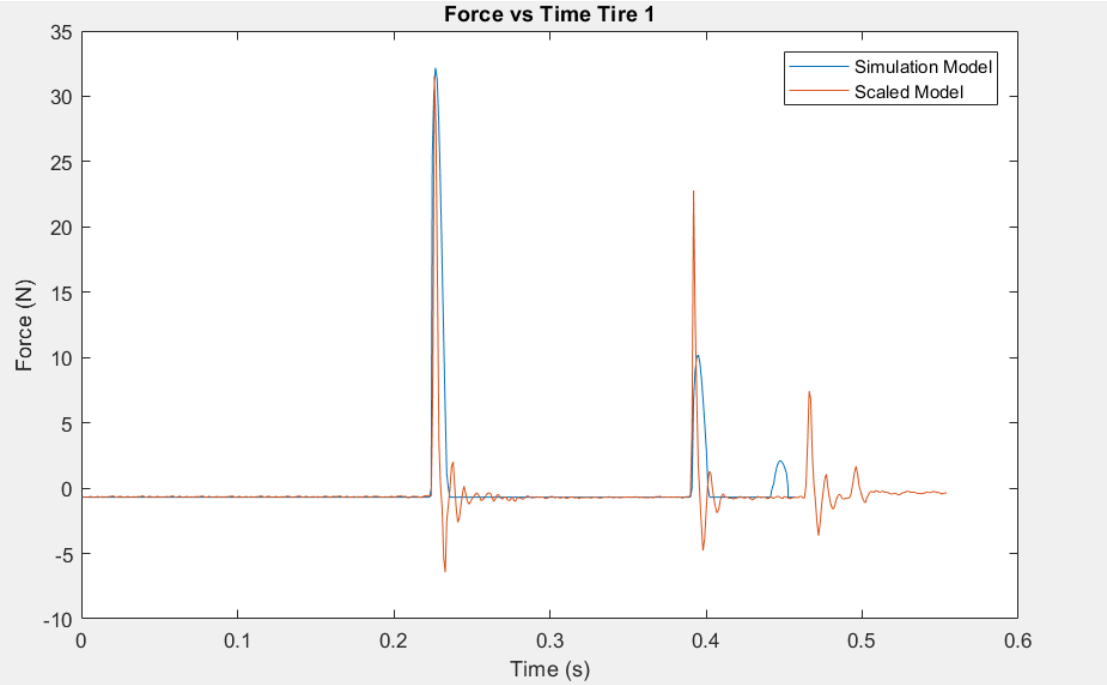

Figure 22. Experimental data and simulation data comparison of first tire

The first peak of the simulation tracks the first impact quite well with a slightly longer predicted impact time. The second peak's amplitude, though, is significantly smaller along with the longer predicted impact time. The three other tires were analyzed in the same way using each of their respective spring stiffness values, as seen in Figures 23, 24, and 25.

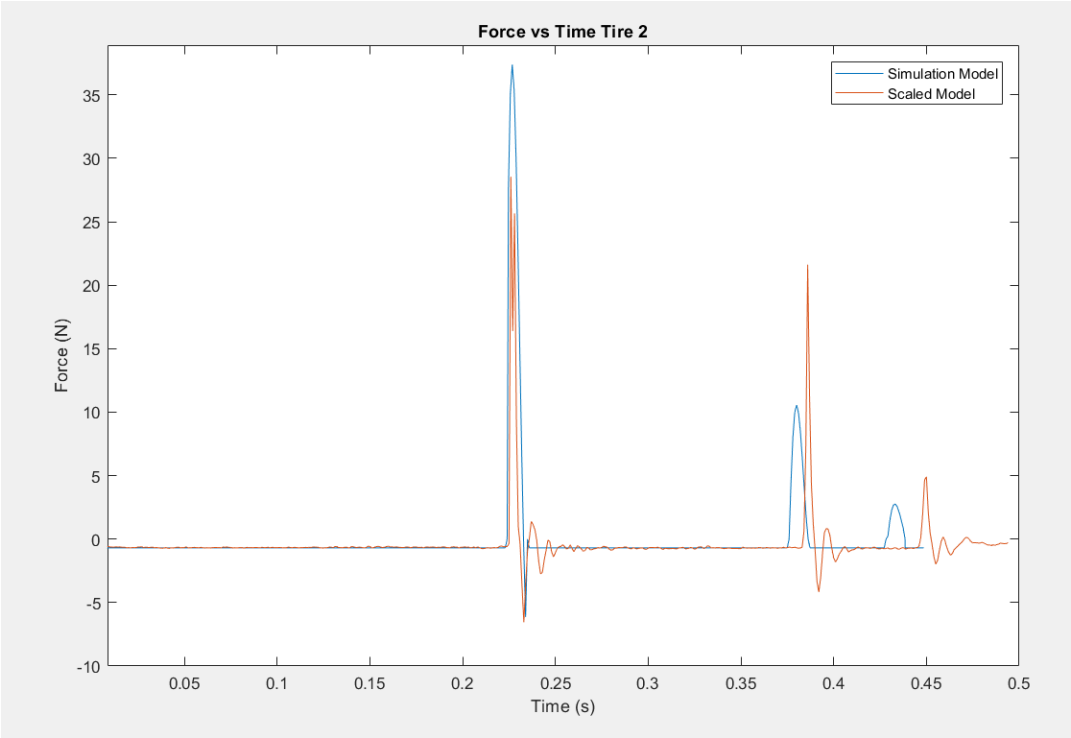

Figure 23. Experimental data and simulation data comparison of second tire

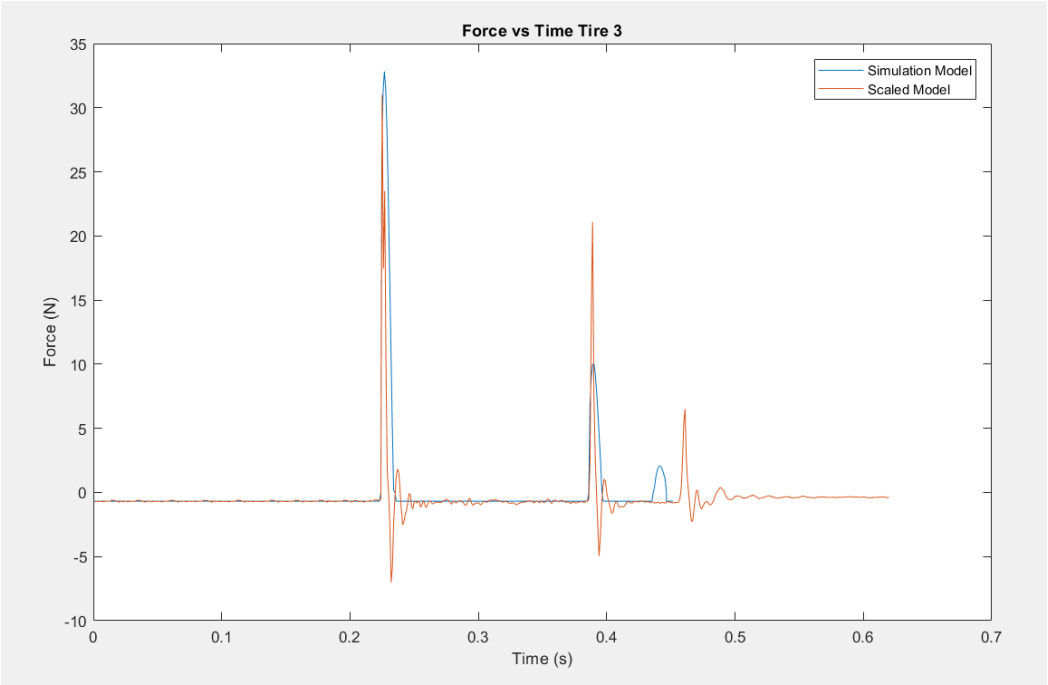

Figure 24. Experimental data and simulation data comparison of third tire

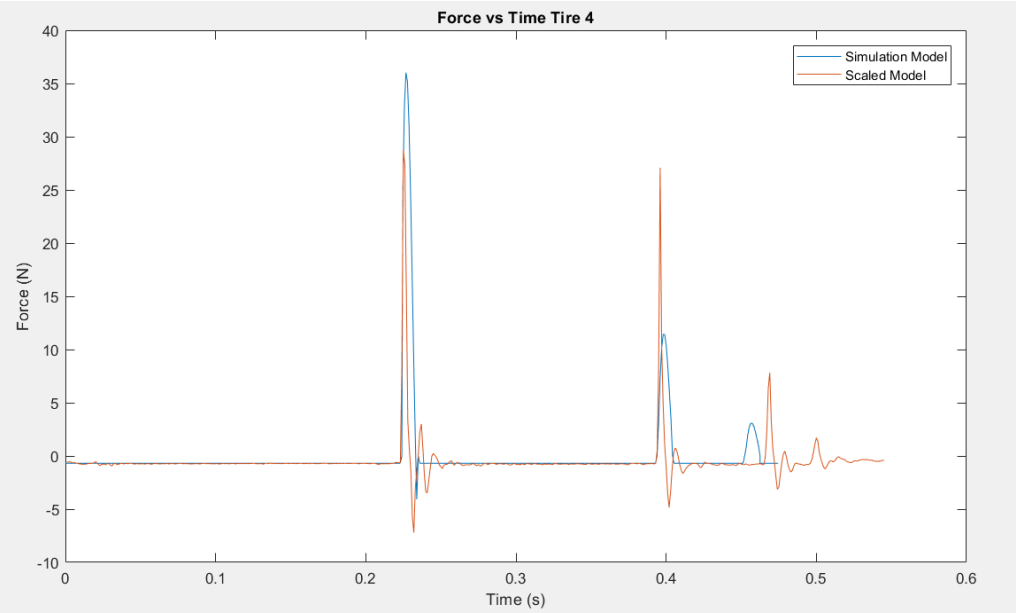

Figure 25. Experimental data and simulation data comparison of fourth tire

Each tire's stiffness and damping value can be seen in Table 7.

Table 7. Tire stiffness and damping coefficients

Tire	1	2	3	4
K (N/m)	5530	7760	5780	7150
B (N*s/m)	14.5	13.8	14.4	14.2

Design of an LCAAT system does not need to consider fatigue, so the main design requirement is for it the system withstand the peak amplitudes. The ratio of the three peak amplitudes of the simulation to the peak amplitude ratios of the experimental data were found and recorded in an Excel file as an **F** scaling vector. This allows the model to adjust for nonlinearities and other factors that would cause distortion if the traditional similitude method was used. A table of the peak amplitude ratios can be found in Table 8.

Table 8. Peak ratios used for F scaling vector

	Tire 1 **F** Vector	Tire 2 **F** Vector	Tire 3 **F** Vector	Tire **4** F Vector
First Peak	0.979	0.756	0.945	0.798
Second Peak	2.54	1.88	2.11	2.36
Third Peak	7.11	1.26	3.12	2.47

5.3 SCALED UP SIMULATION

This section describes a new code, "Bounce_2", that uses new parameter values, the full-size landing gear parameters. While it is difficult to predict the exact values of spring stiffness and damping coefficient, there are some values that can be made based on previous studies.

From section 2.4, the peak experimental force of 14,000 N occurs at a displacement of 0.04 m (Yu, 2014). From this, an approximate stiffness value of 350000 N/m was calculated. The LCAAT drone in question has a maximum weight of 2000 lb. Converting to metric and assuming a tricycle landing gear layout, each gear will support about 300 kg of static load. The effective damping coefficient calculated from Equation 10 gives a value of 1960 N*s/m.

Figure 26 plots the position, velocity, and acceleration returned by the scaled-up simulation using a stiffness value of 350000 N/m, mass of 300 kg, and damping constant of 1960 N*s/m.

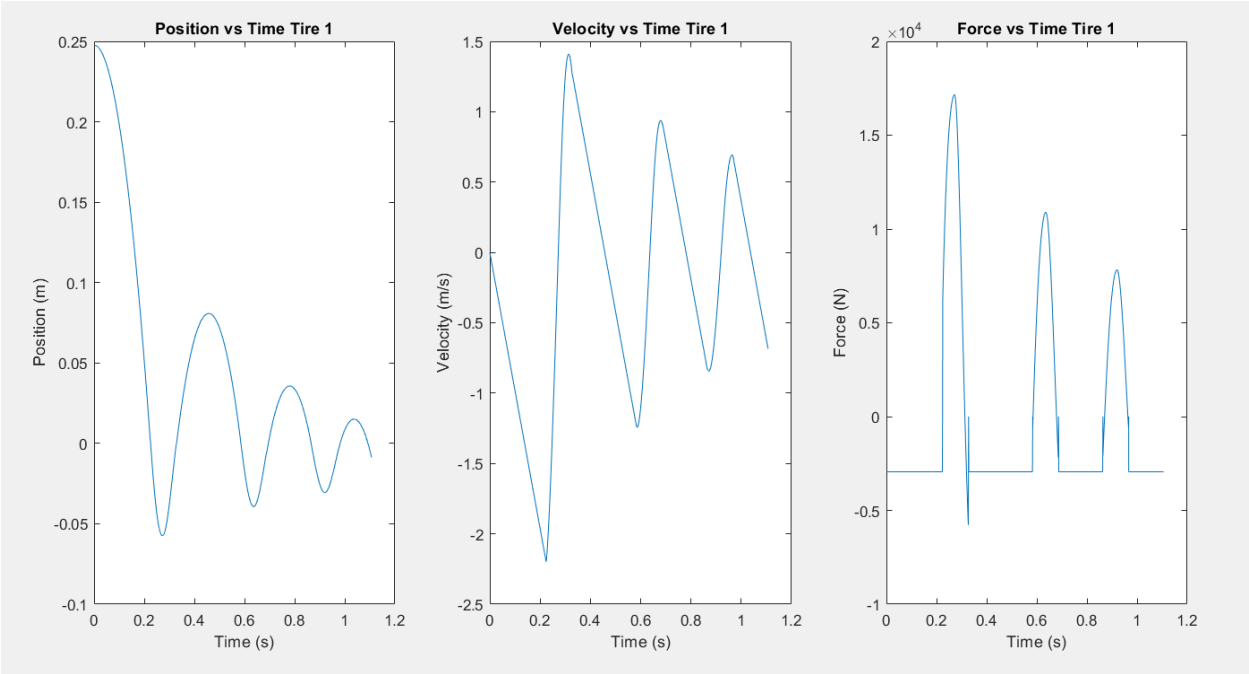

Figure 26. Predicted position, velocity, and force of the product system

It is important to remember that the damping of this system has a quadratic relation with velocity, so this was considered when coding the state equations. The vector **G** is defined as the scaling values of the different properties between the two systems. The ratios of the product to model effective stiffness, effective mass, and effective damping constants were calculated. These ratios of these parameter values became the **G** scaling vector. The scaling values can be seen in Table 9.

Table 9. Parameter value ratios for G scaling vector

	Tire 1 **G** Vector	Tire 2 **G** Vector	Tire 3 **G** Vector	Tire 4 **G** Vector
k_p/k_m	63.3	45.1	60.5	48.9
m_p/m_m	4290	4290	4290	4290
$b_p/(\|v\|*b_m)$	131	143	136	138

Where k_p/k_m is the scaling factor of the full-size landing gear stiffness to the model, m_p/m_m is the scaling factor of the full-size landing gear mass to the experimental drop system mass, and $b_p/(|v|*b_m)$ is the scaling factor of the full-size landing gear to the tire damping factor. The additional $|v|$ term in the damping scale factor is necessary because an oleo-pneumatic system damping is related to the square of the velocity while the tire damping was assumed to be linear.

5.4 Applying Empirical Similitude

Once both **F** and **G** matrices have been calculated, a product can be scaled and compared to actual data of a dropped landing gear system. Due to the associative property of the system, it does not matter which direction is scaled first. Therefore, the simplest path can be chosen. A code was already created with the new parameters, so effectively the new code had been scaled by the **G** vector already. Scaling the peak accelerations of this code by the **F** vector plots is therefore quite simple. In contrast, it would be very difficult to scale the model simulation by the **F** vector first, then try and scale up the physical parameters of the system. Thus, the path of scaling up by the parameter vector, **G**, first and then correcting by the unitless vector, **F** was determined to be the easier and faster route. The response of the original scaled-up system can be seen in Figure 27.

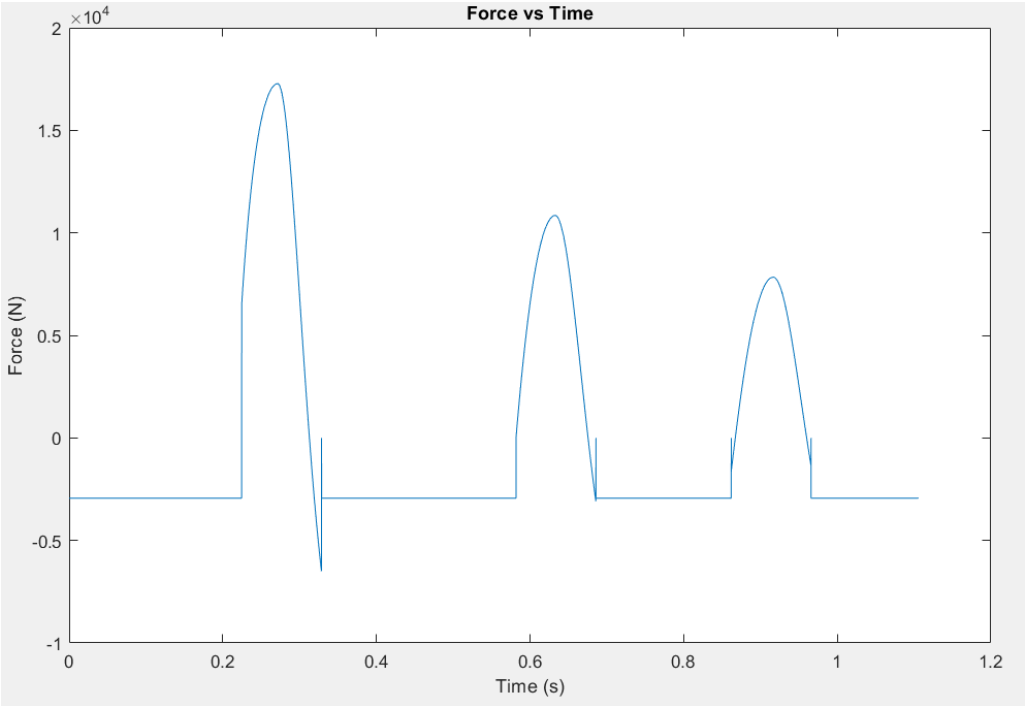

Figure 27. Simulation's predicted force response to dropped landing gear system.

Applying the four **F** matrix scales the bouncing portions by the ratio of the peaks, correcting them to attempt to better match empirical data. Figures 28, 29, 30, and 31 show the comparisons between each of the tires' full size predicted experimental result based on their parameters and the full-size simulation.

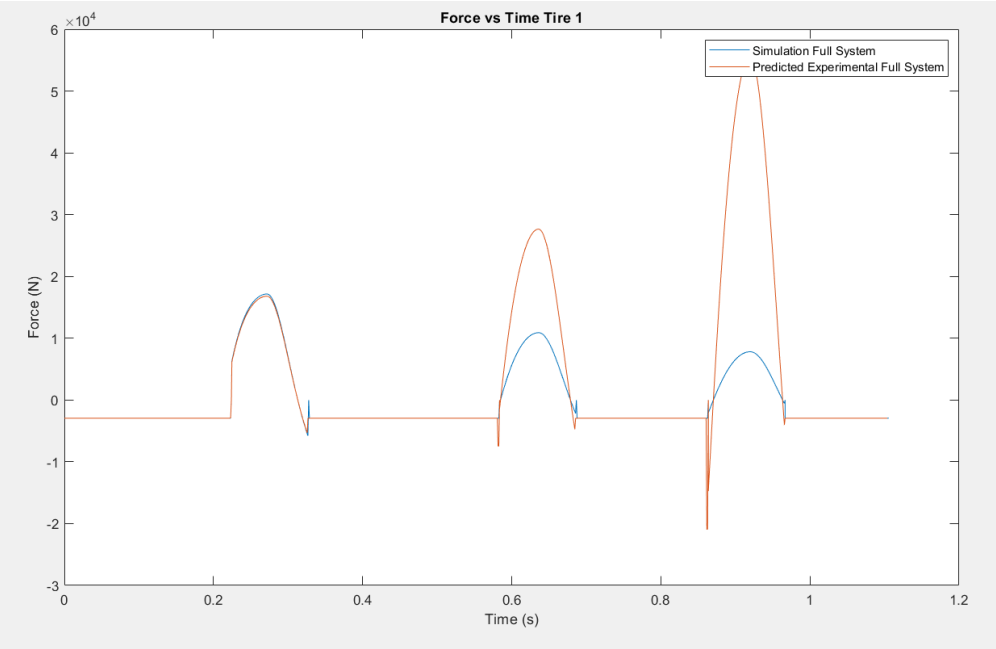

Figure 28. Full size system simulation and predicted force plots of the first tire.

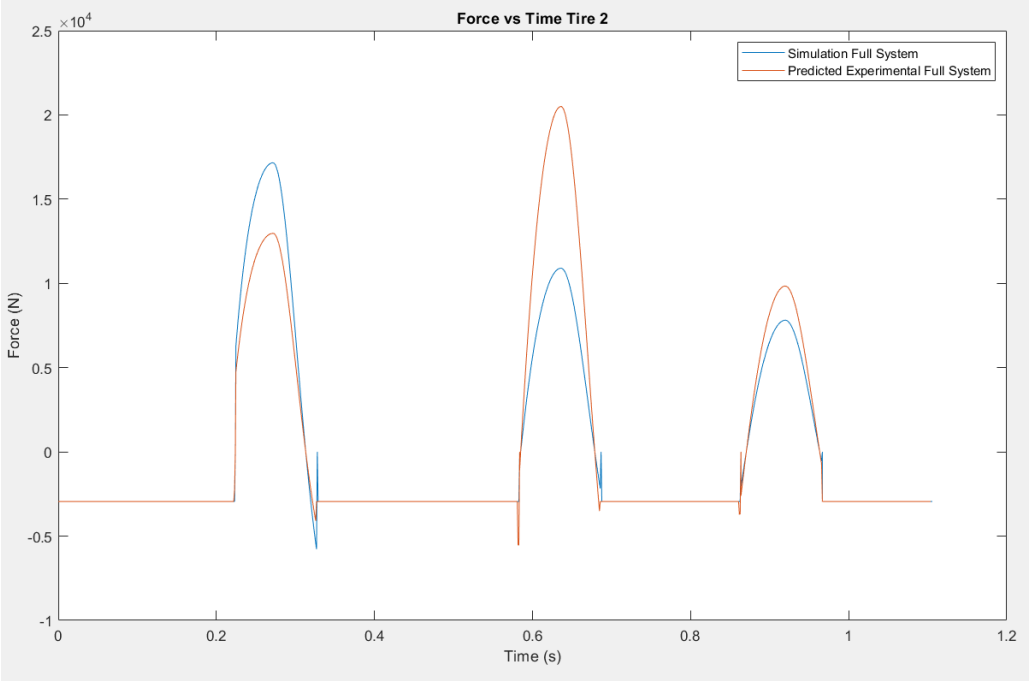

Figure 29. Full size system simulation and predicted force plots of the second tire.

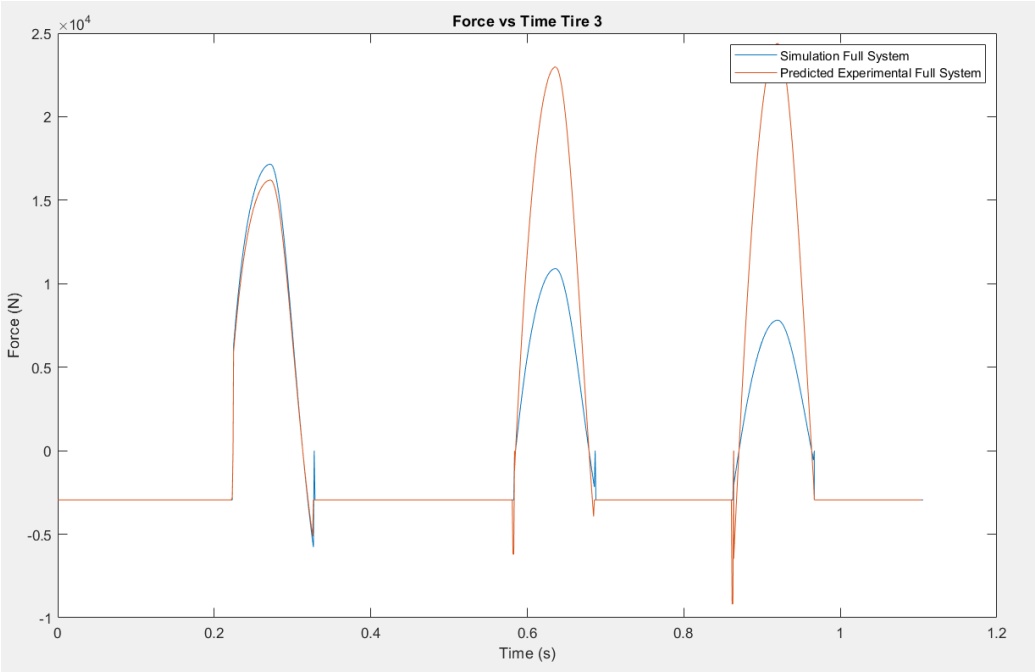

Figure 30. Full size system simulation and predicted force plots of the third tire.

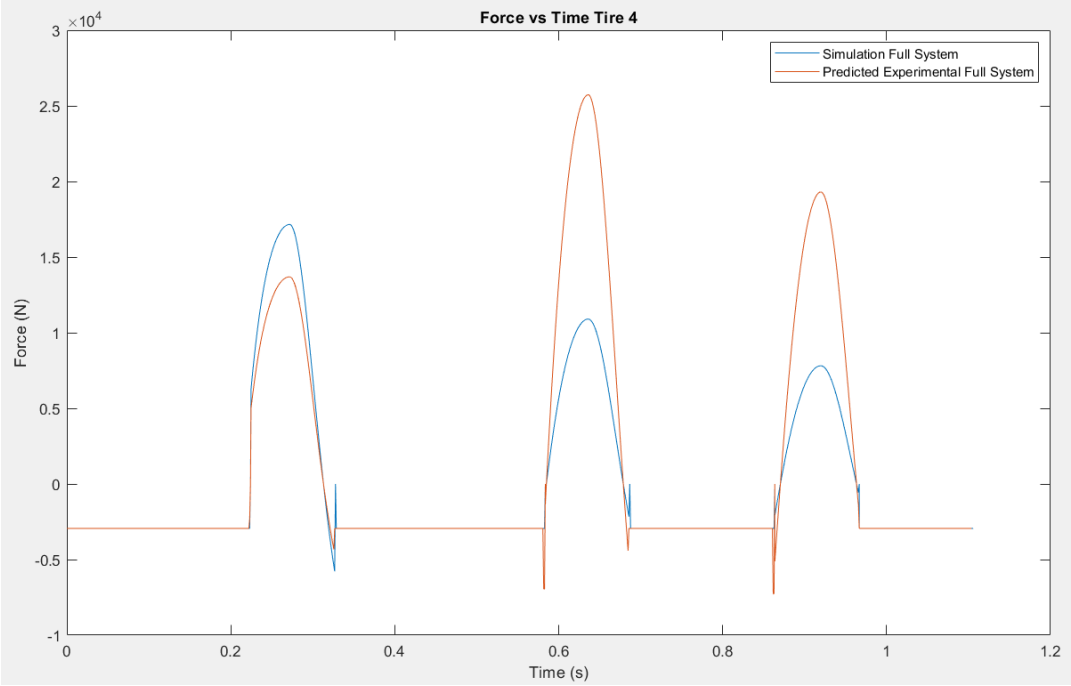

Figure 31. Full size system simulation and predicted force plots of the fourth tire.

5.5 SUMMARY

In this chapter, all the data that was collected was described and presented. Starting with the static tests, the effective stiffness values of the tires were found. Then, the simplified model simulation plots were compared to the empirical data obtained from the dropping tire system. Comparing the peak force values of the simulation to the peak force values of the empirical data, a unitless correction vector, **F**, was formed. Next, stiffness, mass, and damping values for a large landing gear were found. The ratio of these parameter values became the geometric vector, **G**, used for the empirical similitude analysis. Combining these vectors, a final plot was created to analyze in the next chapter.

Chapter 6: Discussion

This chapter discusses the results of the experiments, similitude calculations, and simulations presented in Chapter 4. The goal of this research was to test if applying empirical similitude to the model of an RC landing gear system would be able to predict the response of an oleo-pneumatic landing gear system. Empirical similitude is desired as a guidance for novel design, as testing on a large aircraft is often financially infeasible. If the traditional similitude method was implemented on the smaller system to scale it up, meticulous knowledge of how both the large and small systems work would be required. Instead, empirical data can be used as a tool to more accurately predict responses of the larger system. With two empirical scaling matrices, **F** and **G** defined, the final plots, Figures 27 to 30, show the predicted experimental results after the full empirical similitude system is applied. First, it must be pointed out that the second and third peaks for the predicted experimental results are physically impossible, as they require excess energy be added to the system. The **F** vector shows that for the model system, the experimental data has second and third force peak amplitude values that are twice the size of the ones predicted by the simulation. A study into the accuracy of the quarter car simulation shows that the damping plot for a car spring suspension system is not very linear, but more of a trilinear shape (Maher, 2011). This means that a linear, or quadratic, assumption tends to overestimate the damping constant of the system. There is also looseness in the *x*- and *y*-directions of the experimental setup that could cause the measurements to be inaccurate, especially after the initial impact. While these factors

could account for the error, further study is needed to fully understand why the peak experimental values were underestimated so drastically.

From a system design standpoint, however, the second and third bounces matter less than the initial impact. It is guaranteed that the first impact will be the largest one. This fact, along with the concept that fatigue is not a factor in LCAAT systems means that the first impact is the worst case that should be the focus of system design. For this reason, during analysis the two smaller bounces were ignored. With that, completely new plots of forces focused on the time frame of the initial bounce were generated and can be seen in Figures 32, 33, 34, and 35.

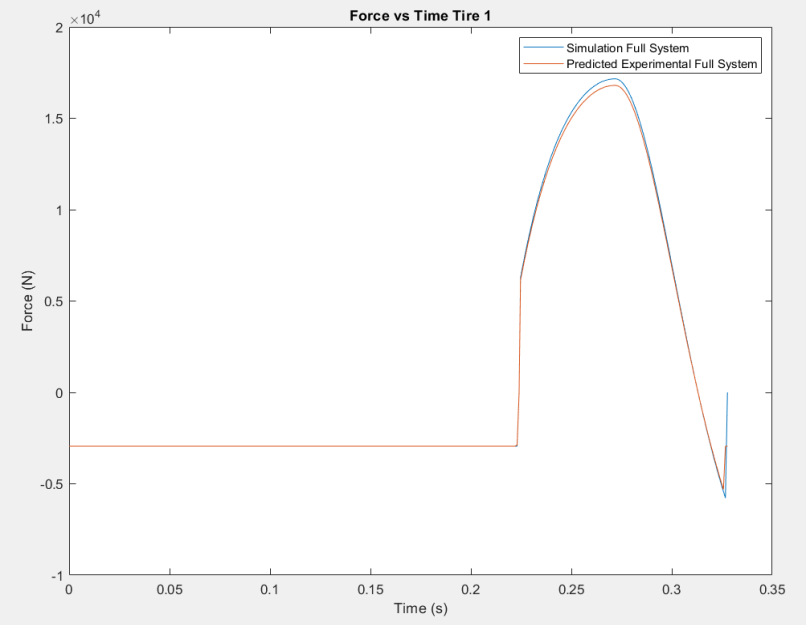

Figure 32. Full size system simulation and predicted force plots of the first tire for the first bounce.

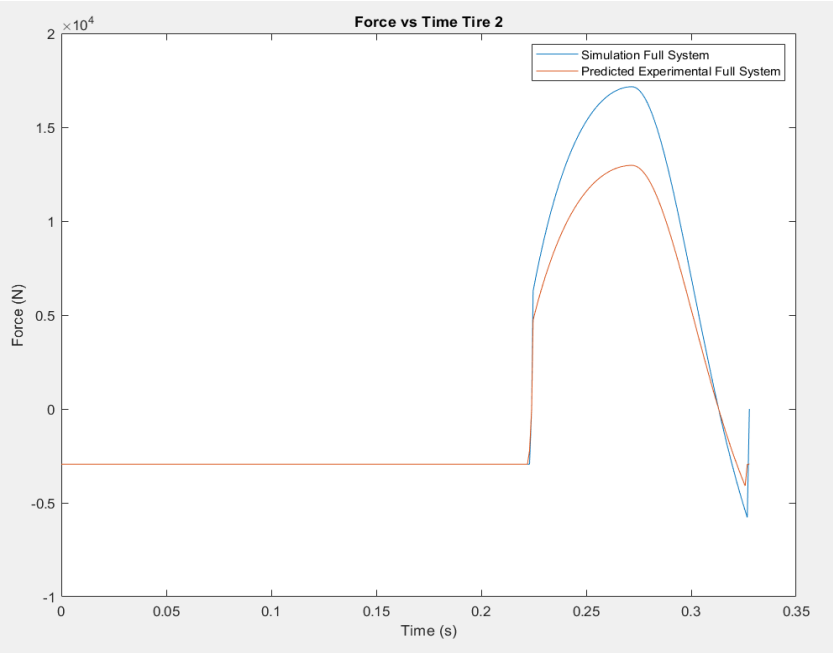

Figure 33. Full size system simulation and predicted force plots of the first tire for the second bounce.

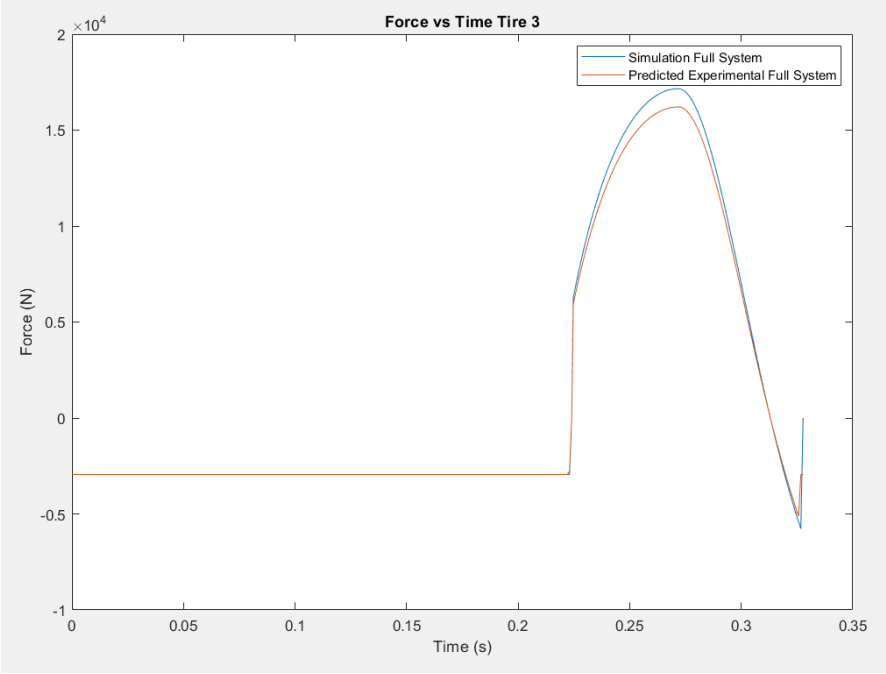

Figure 34. Full size system simulation and predicted force plots of the first tire for the third bounce.

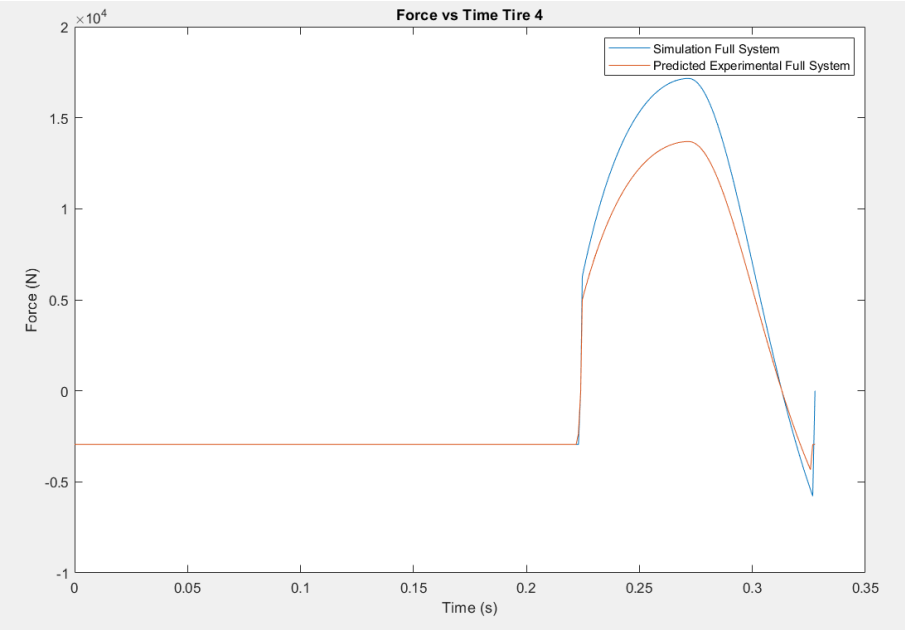

Figure 35. Full size system simulation and predicted force plots of the first tire for the fourth bounce.

Figure 35 shows the peak forces of a previously tested full-size landing gear.

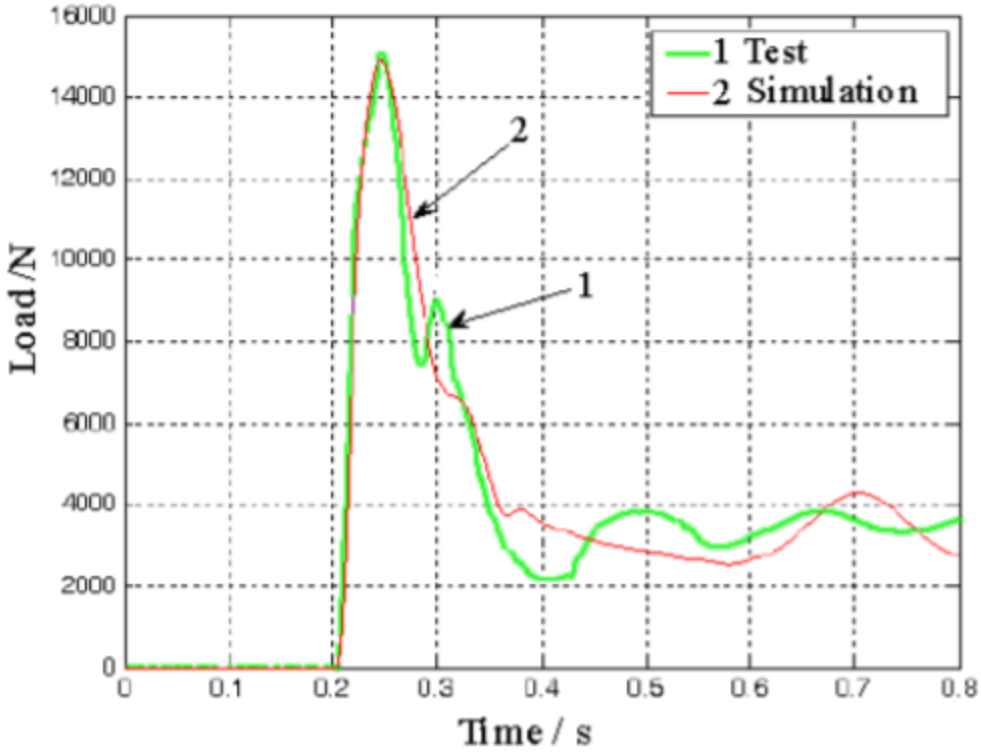

Figure 36. Force vs. Time experimental data and simulation response of a full-size landing gear system (Yu, 2014)

Comparing Figures 31, 32, 33, and 34 to Figure 35, tires 2 and 4, which have higher stiffness values, gave fairly similar results, with a maximum impact of about 15000 N. The timing difference can be attributed to the slight difference in drop height, pushing the impact time back about 0.25 s. There is also a second peak that is difficult to explain in the experimental data, possibly due to vibration of the system after the impact. For the purposes of this study, this second peak was ignored.

Another important difference between the empirically derived model and the experimentally derived plot is the experimental plot goes straight to vibration after the

initial impact while the empirical model predicts the system bounces into the air. This is most likely due to larger damping and mass as these were difficult to find for the experimental system. Since the design focuses on peak impact, this difference can be ignored as well.

There is a drastic difference in accuracy depending on the initial spring stiffness value. The small tires are packaged in pairs, meaning each set of two tires will likely have similar properties. Without further testing, it is difficult to determine the full range of stiffness values of the tires. With the current data, the values tend to be conservative and overestimate the force on the full landing gear. This means that this model, while not necessarily the most accurate, can still be used to design for maximum load on the landing gear system.

Chapter 7: Conclusion

This research shows that the second order ODE model of a bouncing RC plane landing gear system has potential to accurately predict the loads on a full-size oleo-pneumatic landing gear system with accurate empirical data and parameters.

For this work a model system was created for the RC plane using a reverse pendulum to drop the RC plane tire and track its acceleration. This acceleration was used to find the force response on the landing gear system.

A MATLAB program tracking the position, velocity, and force on the model landing gear system was built and compared to the empirical data. Tire mass and static stiffness were measured and used for each of the four tires, while the damping constant was found by matching the second and third times of impact. The ratio between the peak impacts created the unitless matrix **F** used for the empirical similitude process.

The code was then scaled up using parameters calculated from a full-size drop test system. The scaling vector created by the ratio of parameters was called the geometric **G** matrix in the empirical similitude process.

Applying both **F** and **G** matrices, the results of the empirical similitude were compared to known peak data values from literature. The values tend to be either reasonably accurate or very conservative, overestimating peak force of the initial impact. The second and third impact responses of the full-scale system, after empirical similitude application, were determined to be physically impossible. Due to the low cycle criterion

of the LCAAT system, however, these peaks can be ignored for the peak impact load when designing the system.

7.1 RECOMMENDATIONS

While there were some values that matched empirical data from literature after the model system was scaled by empirical similitude, it is recommended that more tires be tested to find a more accurate static stiffness value. It is also recommended that the second and third bounces be examined in more detail to determine why the predicted response is about half of the model system empirical response. Lastly, while literature is a good source for preliminary testing, drop testing a full-size landing gear system and using that data instead of literature data would allow for more control over the scaling matrices. This in turn would create opportunities to test the limitations of the effects of empirical similitude.

References

All Modern. (2002). *Derouen Dining Table*. Retrieved from: https://www.allmodern.com/furniture/pdp/derouen-dining-table-vrkg1767.html.

Bauer, P. (2014). "A Simple Landing Gear Simulation Model for Unmanned Aerial Vehicles". *Periodica Polytechnica*. 42(1). pp. 11-18.

Crossbow Technologies (n.d.). Accelerometers: General Purpose LP Series. *Datasheet Archive*. Retrieved from http://www.datasheetarchive.com.

Davidson, G. W. (2015). Improved Landing Gear Shimmy Model. *SAE International*. 8(1). pp. 150-154.

Dutson, A. J. (2002). Functional Prototyping Through Advanced Similitude Techniques (Doctoral dissertation). Available from Texas ScholarWorks.

Gudmundsson, S. (2014). *General Aviation Aircraft Design: Applied Methods and Procedures*. Waltham, MA: Elsevier Inc.

Gundlach, J. (2014). *Designing Unmanned Aircraft Systems: A Comprehensive Approach*. Manassas, VA: American Institute of Aeronautics and Astronautics, Inc.

Khondker, M., Kabir, L., Younes, A., Shelimuzzaman, M., Islam, S. (2009). Landing Gear Shock Absorber Design. [Presentation]. *Powerpoint presented to Dr. S.V. Hoa at Concordia University*. Austin, TX.

Kypuros, J. A. (2017). *Inverted Pendulum Control System*. Retrieved from: http://dsc.utrgv.edu/VirtualLab/Pendulum/Pendulum.html.

Maher, D., & Young, P. (2011). *An insight into linear quarter car model accuracy*. Vehicle System Dynamics. 49(3). 463-480.

Murphy, Glenn. (1950). *Similitude in Engineering*. NY: Ronald Press Co.

Risma, C., Nair, N., Bradley, N., Fernandez, N., Porter, E. (2016). Launch and Recovery of Low Cost Attritable Aircraft Technology (LCAAT). [Presentation]. *Lecture given to Cadets of the United States Air Force Academy*. Colorado Springs, CO.

Sayyad, A. S. (2011). Comparison of various refined beam theories for the bending and free vibration analysis of thick beams. *Applied and Computational Mechanics*. 5. pp. 217-230.

Shell. (2012). "AeroShell Book". Shell Global. Retrieved from https://www.shell.com/business-customers/aviation/aeroshell/knowledge-centre/the-aeroshell-book.html.

Shrotri, K. (2008). Composite Skid Landing Gear Design Investigation (Doctoral dissertation). Available at the School of Aerospace Engineering Georgia Institute of Technology.

Sutherland, J. W. (2004). An Introduction to Mechanical Vibration. Retrieved from: http://www.mfg.mtu.edu/cyberman/machtool/machtool/vibration/intro.html.

United States Air Force Academy. (2016). Cadet Information. Retrieved from USAFA website http://www.usafa.af.mil/About-Us/Cadet-Information/

Yu, J. W., Liu, X. F., Wang, H. L., Wei, Y. J. (2014). Dynamic Characteristics of Aircraft Landing Gear. *Applied Mechanics and Materials*. 543-547. pp. 118-121.